Scattered Gamma Rays From Thick Uranium Sources

GEOLOGICAL SURVEY BULLETIN 1052-A

Scattered Gamma Rays From Thick Uranium Sources

By A. Y. SAKAKURA

EXPERIMENTAL AND THEORETICAL GEOPHYSICS

GEOLOGICAL SURVEY BULLETIN 1052-A

UNITED STATES GOVERNMENT PRINTING OFFICE, WASHINGTON : 1957

UNITED STATES DEPARTMENT OF THE INTERIOR

FRED A. SEATON, *Secretary*

GEOLOGICAL SURVEY

Thomas B. Nolan, *Director*

For sale by the Superintendent of Documents, U. S. Government Printing Office
Washington 25, D. C. - Price 25 cents (paper cover)

CONTENTS

ILLUSTRATIONS

TABLES

LETTER SYMBOLS

A=area of elementary source
A_0=area of standard elementary source=1,600 ft^2
a=radius (or width) of source
H_f=area under curve recorded over finite source by counting-rate meter
H_l=area under curve recorded over line source by counting-rate meter
H_p=area under curve recorded over elementary source by counting-rate meter
H_s=area under curve recorded over slab source by counting-rate meter
I_b=intensity from broad source
I_f=intensity from finite source
I_l=intensity from line source
I_p=intensity from elementary source
I_s=intensity from slab source
R=response of counting rate meter
r=air distance between source and detector
S=grade of source in equivalent uranium
S_0=grade of standard source in equivalent uranium=0.35 percent U
t_0=time the source first falls within cone of response of detector
x=altitude of detector above source plane
y=source plane projection of the air distance from the detector to source center line
z=ground projection of distance of closest approach of detector to source
α=½ angle of cone of response of detector
β=distance traveled in one time constant in mean free paths
θ=angle determined by relative displacement of peaks on two adjacent lines
μ=linear absorption coefficient of the most penetrating gamma ray of the U spectrum=1.46×10^{-3} ft at sea level
ρ=projection on the source plane of the air distance from detector to center of finite source
τ=time constant of detector

EXPERIMENTAL AND THEORETICAL GEOPHYSICS

SCATTERED GAMMA RAYS FROM THICK URANIUM SOURCES

By A. Y. Sakakura

ABSTRACT

Semiquantitative interpretation of data from airborne radioactivity surveying requires detailed knowledge of scattered gamma-ray intensity at considerable air distances from natural thick uranium sources. Based on the concept of an elementary source of infinite thickness rather than a conventional point source, empirical expressions, which are of the form dictated by theory, are developed for measured gamma-ray intensities from two extreme types of natural uranium sources, the elementary and the broad source. Computation, based on published solutions of the Boltzmann equation for gamma-ray transport in one medium, is in agreement with experimental measurements. The calculated value for primary, scattered, and total intensities from thick uranium sources show that at considerable air distances the scattered intensities are more than half of the total intensity for energies above 0.4 Mev and become much more than half as the lower limit of detector energy response is decreased below 0.4 Mev.

From the expression for the gamma-ray intensity of elementary source, gamma-ray intensities from idealized sources, selected to approximate most nearly naturally occurring sources, have been computed. All computations are based on the assumptions of quarter-mile flight line spacing, and flight path at 500 feet above ground at atmospheric pressure. The computed data are strictly valid only for these conditions of airborne radioactivity surveying and for scintillation detectors of essentially identical spectral energy response.

The intensities and areas under the curve that would be recorded by a counting-rate meter have been computed for selected source types, the elementary, the finite, the slab, the line, and the broad source. The peak intensity and the area under the curve are the two interrelated observable quantities most useful for interpretation. The shape of recorded anomalies as shown by analysis of experimental and computed data cannot be used for interpreting grade-area and (or) grade of natural sources although shape is useful in determining source type.

In interpreting anomalies, 4 of the 5 source types can be distinguished by the appearance of an anomaly, either on one or on two or more adjacent flight lines; one type, the broad source, can be readily distinguished by flattening of the anomaly on adjacent flight lines. With source type identified, the grade-area and (or) grade of a natural source can be determined from tabulated data for the two observable quantities, the peak intensity and the area under the curve. The accuracy of interpretation of grade of broad and slab sources has been confirmed by field investigations; the interpretation of grade-area and (or) grade of

finite and elementary sources, particularly those visible on only one flight line, is difficult and is satisfactory only within an order of magnitude.

The method of interpretation, based on a semiempirical approach, is applicable to measurements made with scintillation detectors of broad spectral energy response. For other than essentially identical radiation detection instruments, the necessary constants which specify the buildup factor for any specific detector can be established by empirical tests of the response to known thick uranium sources.

INTRODUCTION

Airborne radioactivity surveying is now widely and successfully used, primarily to prospect for uranium. In the majority of airborne surveys the sought-for target is a radioactivity anomaly, a sharp local increase in radiation intensity. Data on anomalies are usually reported on a qualitative basis (Stead, 1955).

To advance airborne surveying from the qualitative to the semiquantitative estimation of natural-source parameters, a greater knowledge of air-scattered gamma-ray intensity at considerable air distances from naturally occurring thick uranium sources is necessary. The scope of the knowledge must be such that for any specific instrument of gamma-ray detection and measurement the observable data for a given anomaly, such as the peak intensity, the area under the curve, and the shape of the curve, can be correlated with the principal characteristics of a natural source, namely the strengh in terms of the equivalent uranium oxide content and the configuration in terms of the surface dimensions.

Inasmuch as naturally occurring sources are usually poorly defined in area and composition, and the radiation effects are obscured by surrounding sources, a purely empirical study would present great difficulties in determining the salient features of the radiation intensity from a given source type. It therefore seems more practicable to investigate numerically and analytically the features of certain simple source types, never found in nature, but nevertheless covering the entire range of variation in shape and size found in natural sources.

The following sequence of action presents itself:

Determination of the radiation intensity, theoretically or experimentally, from an elementary source from which other sources can be constructed.

Determination of the radiation intensity from simple sources by distribution of the elementary source over suitable geometrical configurations.

Investigation of the relationship between the source characteristics, such as size, grade, shape, and the observable data such as peak intensity reading and area under the counting-rate meter curve for several sources to establish criteria for distinguishing the different source types.

Relation of source characteristic directly to the observable data without reference to (unknown) distance, with the criteria for distinguishing source types established.

Reduction of information gained in the previous steps to a simple recipe suitable for actual field applications.

This report is devoted primarily to the establishment of the expression for the elementary-source intensity, to a comparison of experimental results with existing theoretical knowledge, and to the effect on the apparent peak intensity of the finite cone of response and resolving time of a counting-rate meter. Characteristics of selected source types are established and a possible mode of interpreting airborne radioactivity measurements in terms of natural-source parameters is outlined.

ACKNOWLEDGMENTS

The writer is deeply grateful to L. V. Spencer, of the National Bureau of Standards, for a long enlightening discussion on the nature of gamma-ray scattering and on the format and contents of the paper. The section entitled "Comparison with theory" was inserted upon his suggestion. The writer is also grateful to F. J. Davis, of Oak Ridge National Laboratory, who compiled most of the data and to R. H. Ritchie, of Oak Ridge National Laboratory for many fruitful discussions. He is indebted to N. Lazar of Oak Ridge National Laboratory for determining the equilibrium spectrum of uranium.

The work herein reported is part of an investigation carried on by the U. S. Geological Survey on behalf of the Division of Research of the U. S. Atomic Energy Commission.

GAMMA-RAY INTENSITY FROM ELEMENTARY AND BROAD SOURCES

DETERMINATION OF EMPIRICAL RELATIONS

As the fundamental properties of gamma radiation are well known for the energy range observed in natural sources, the ideal method of interpretation would be based on theoretical computation of the radiation intensity emanating from several sources, by solving the Boltzmann equation for gamma-ray transport in two-media. This solution, in general, is a function of three space variables, two angular variables and an energy variable. The advantage of the computational approach is that the results do not have to be resolved in terms of the response characteristics of a particular detector, and that the response of any detector, if its spectral and angular characteristics are known, can be computed. No satisfactory solutions to the general two-media problems have yet been published, although the U. S. Geological Survey and the Atomic Energy Commission Computing Facility at New York University are now engaged in solving the two-media

problems with plane symmetry. However, Fano (1953a, 1953b) and Spencer and Fano (1951) have made extensive analytical studies, and a vast quantity of numerical solutions to one-medium problems in plane and spherical geometry exists (Goldstein and Wilkins 1954), from which one may predict trends of solutions in two-media problems. Moreover, for moderate energy gamma rays, two-media problems with plane symmetry can be reduced to equivalent one-medium problems. The general procedure for solving the Boltzmann equation was developed by Spencer and Fano. A topical summary and pertinent bibliography can be found in recent articles by Fano (1953a, 1953b).

However, the simplest approach is a semiempirical one, wherein an experimentally determined or assumed form of radiation-intensity law for an elementary source is integrated over a suitable geometric configuration to obtain the intensities from various sources. Peirson and Franklin (1951) performed such an integration assuming an inverse-square exponential law which not only neglects the effect of scattering but also the multitudinous lines of the uranium gamma-ray spectrum. Carmichael and others (Steljes and others, 1952) used the inverse-square law but took air scattering into account by experimentally determining the "effective absorption coefficient" by measuring the radiation from radium sources. Cook (1952) assumed an "effective" energy and utilized "effective" computed cross-section and the inverse-square law. However, there is no priori reason why any "effective" quantity computed or measured in one source-to-medium orientation should be applicable to others. To avoid this difficulty measurements were made on infinitely thick sources, wherein the integration in depth is already performed in the data, and the different sources are synthesized through integration over a suitable surface.

Although the empirical approach was chosen for simplicity, it is useful to retain the form and the structure predicted by theory for the purpose of extrapolation into areas not covered by the data. Then, the radiation intensity will take the form of the product of the most penetrating primary component and a buildup factor, a polynomial in the distance variable for the case of moderate penetration (Fano, 1953a; Spencer, and Fano 1951).

There are two extremes in source types found in nature. One of them, which will be called an elementary source, from which every other source can be computed by integration, is depicted in figure 1, an infinite line embedded in the ground. The other extreme, which will be called a broad source, is depicted in figure 2, a half space uniformly filled with radioactive matter. It is obvious that the second

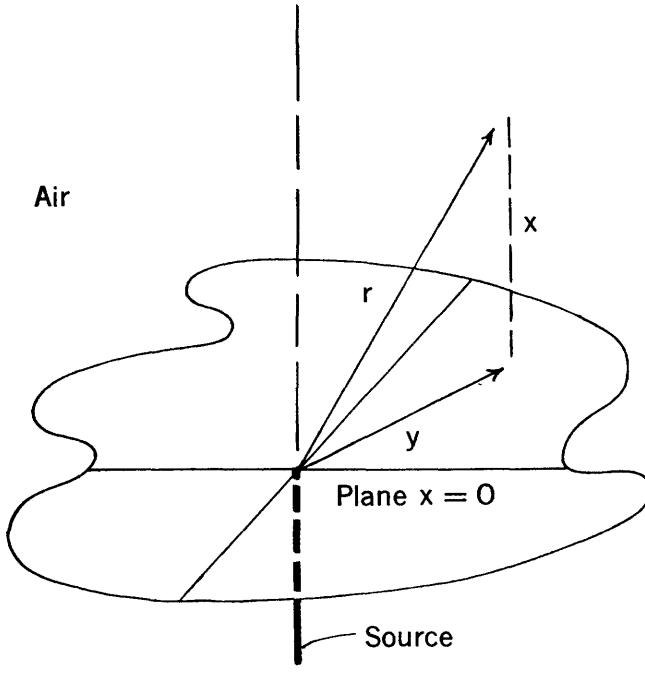

FIGURE 1.—Elementary-source geometry.

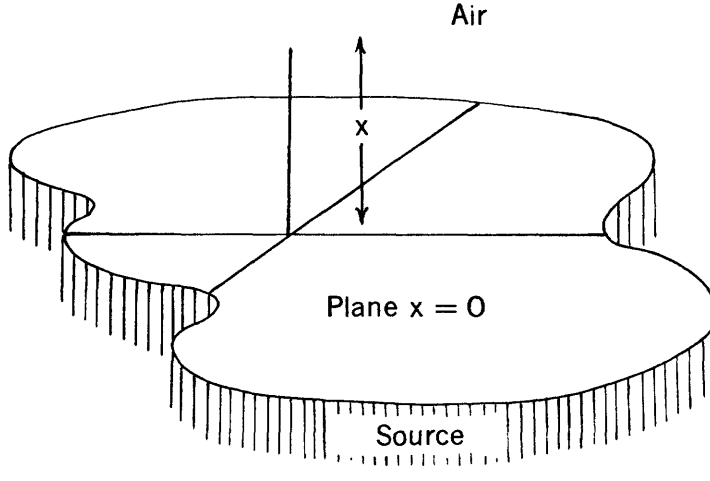

FIGURE 2.—Broad-source geometry.

source can be formed by infinite superposition of the former. Thus an empirical form chosen for the elementary source should be such that it not only fits the elementary-source data, but also, when integrated over an infinite area, should fit the broad-source data. In this manner, any intermediate form of sources should be well represented by the integration of the elementary source over a suitable geometrical configuration.

In this section, empirical expressions will be established for the elementary and the broad sources. It is known that the radiation intensity can be written as a product of two factors, one representing the primary contribution from the unscattered components, and the other, a buildup factor representing the contribution from scattered radiation (Fano, 1953a, 1953b; Spencer and Fano, 1951). The latter factor is generally a polynomial for moderate penetration.

An extensive series of experimental measurements to provide statistically sound data bearing an absorption and scattering of gamma radiation was planned and completed in cooperation with the Health Physics Division of the Oak Ridge National Laboratory. Measurements were made at different altitudes above a simulated elementary source and an infinite broad source with scintillation detection equipment designed and constructed by Oak Ridge National Laboratory and installed in a multiengine airplane.

The simulated elementary source is at Walker Airport, Grand Junction, Colo., and consists of a slab of carnotite ore 40 feet square and 6 inches thick sealed by a thin rubberized fabric to minimize escape of radon. The source contains 48 tons of ore at 0.35 percent U_3O_8 (1.31×10^3 gU and 47.1 mg Ra).

In comparison with the infinitely thick source, the 6-inch thickness or ore yields 95 percent of the primary intensity of the most abundant gamma ray (0.609 Mev) and 75 percent of the intensity of the most penetrating gamma ray (2.432 Mev). The areal extent of the simulated source is small enough to be considered an elementary source at air distances several times greater than the effective diameter of the slab.

The experimental measurements over the source were made at 100-foot spacings from 100 to 800 feet above the ground both directly over the source and at horizontal distances from the center-line to one side of the source, of 125, 250, 375, and 500 feet. The flight level of the aircraft was determined by a continuously recording radio altimeter. Flight-line markers for pilot guidance were set up across and parallel to the source with one line of grid markers through the source and perpendicular to the flight-line markers. A gyrostabilized continuous-strip-film camera recorded each flight; thus, from the known focal length of the lens, the distance from the ground and also the

horizontal distance offside the source could be calculated within about 10 feet. The nominal flight levels as determined by the radio altimeter were often in error by as much as 80 feet when compared with the more accurate determinations of position based on the continuous-strip photograph.

In figure 3 the net counting rates from a broad source at minimum pulse height acceptance levels corresponding to 0.05, 0.1, 0.2, and 0.4 Mev are plotted against altitude above the source. Each point corresponds to the average of five readings taken by three observers. The solid lines correspond to exponential curves fitted by least squares.

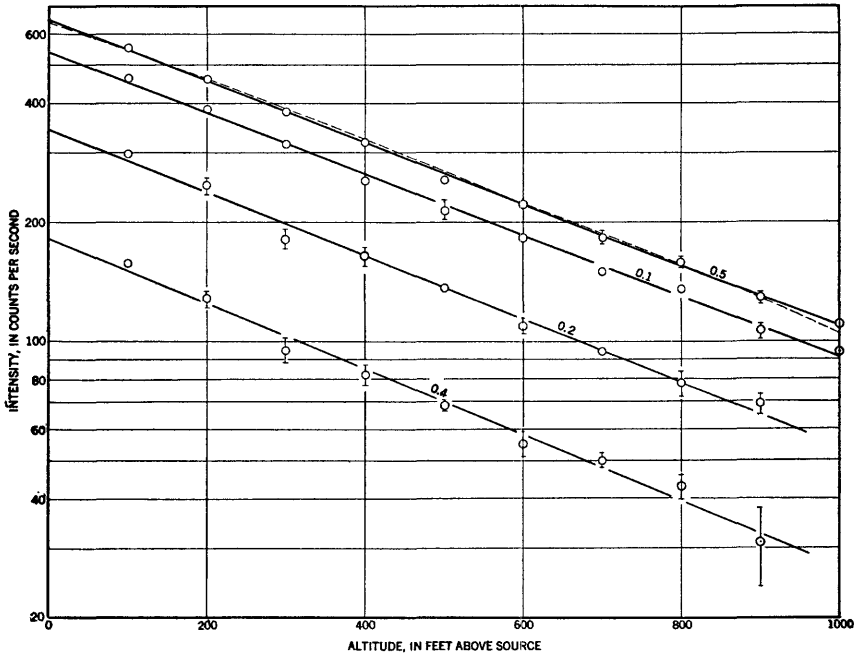

FIGURE 3.—Broad-source data.

The slopes are constant, and consequently it is concluded that within the limits of experimental error, the spectral composition does not change. Consequently, all further measurements and considerations are based on the highest counting rate, corresponding to the lower energy acceptance level of 0.05 Mev.

The broad source is near Fruita, Colo., an area of Mancos shale several square miles and of farily uniform composition. Representative trench samples of the shale contained 1.6 percent K, 0.0017 percent U (fluorimetric), and 0.0013 percent equivalent U. Experimental measurements over the source were made at 100-foot spacings from 100 to 1,000 feet above the ground.

The elementary-source intensity, Ip, is expressed as

$$Ip\ (x,\ \rho)=\frac{CSA}{S_oA_o}\frac{x}{r}\frac{e^{-\mu_o r}}{r^2}\left[1+a_1\ (\mu_o r)+a_2\ (\mu_o r)^2\right] \tag{1}$$

where

x = altitude of detector above source plane
ρ = projection on the source plane of the air distance from source to detector
r = air distance $=\sqrt{x^2+\rho^2}$
C, a_1a_2 = constants to be determined
A = area of an elementary source
A_o = area of standard elementary source = 1600 ft^2
S = grade in eU of source
S_o = grade in eU of standard source = 0.35 percent U
μ_o = linear absorption coefficient of the most penetrating gamma ray of the U spectrum $=1.46\times10^{-3}$ ft^{-1} at sea level

The factor x/r is the effective area of the source as "seen" by the detector (fig. 1). Because of the strongly absorbing nature of ground only the gamma rays from a finite depth of an infinitely thick source contribute appreciably to the counting rate. The next factor, $\frac{e^{-\mu_o r}}{r^2}$, is the primary intensity from the most penetrating component. The square bracketed factor is the buildup factor which is not identical to the buildup factor of theory, as it also includes the effects of more rapidly decaying exponentials of the less penetrating primary components.

The intensity from a broad source, $I_b(x)$, is

$$\begin{aligned} I_b(x)&=2\pi\int_o^\infty \rho\frac{I_p(x,\ \rho)\ d\rho}{A}\\ &=\frac{2\pi\ CS}{S_oA_o}\left\{\left[1+a_2\mu_o x\right]\ e^{-\mu_o x}+(1-a_1)\mu_o x\int_x^\infty\frac{e^{-\mu_o r}}{r}dr\right\} \end{aligned} \tag{2}$$

As these equations are largely arbitrary, and for the sake of retaining simple equations, a_1 is taken to be 1. Thus

$$I_p(x,\rho)=\frac{CSA}{S_oA_o}\frac{x}{r}\frac{e^{-\mu_o r}}{r^2}\left[1+\mu_o r+a_2(\mu_o r)^2\right] \tag{3}$$

$$I_b(x)=\frac{2\pi\ CS}{S_0A_0}e^{-\mu_o x}\left[1+a_2\ (\mu_0 x)\right] \tag{4}$$

These are the equations to be fitted to the data.

Simple exponential inverse-square expression for a point source such as those given in Peirson and Franklin (1951), will yield, with the use of a linear build-up factor, exponential broad-source expression upon integration over an infinite half space. Whereas such an expres-

sion can represent the broad-source data adequately, the inverse-square-exponential point-source expression, multiplied by a linear build-up factor and integrated over a semi-infinite line, fails to fit the data for the elementary source. Thus, equation (3) should be used in defining the expression for the elementary-source intensity. Moreover, as the two sources are the extremes in the geometrical configuration of the source rock, the evaluation of the constants by using the data from both sources would yield an expression for the elementary-source intensity most suitable for superposition into arbitrary sources.

The dotted line curve (fig. 3) represents the expression

$$I_b(x) = (638 - 218\mu_o x)e^{-\mu_o x} \tag{5}$$

which was fitted by least squares to the broad source data, from which is obtained the value, -0.342 for a_2 from the broad source data. With a_2 established, it remains merely to determine C. In figure 4,

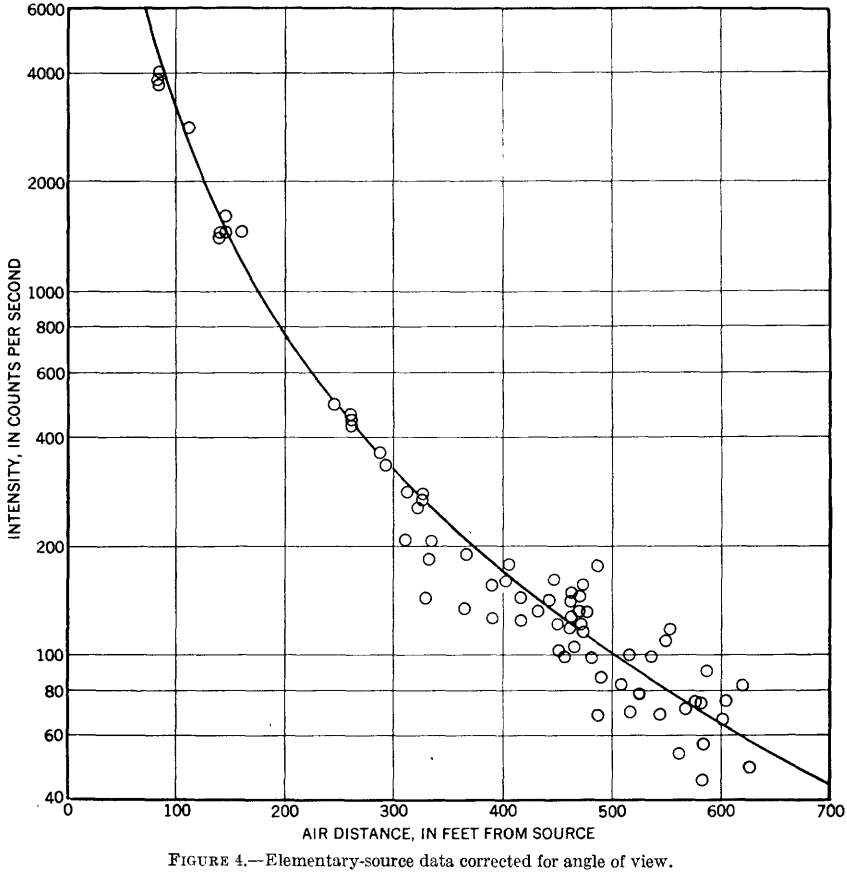

FIGURE 4.—Elementary-source data corrected for angle of view.

the data for the elementary source, corrected by the factor r/x, are plotted against air distance r. The expression defined in equation (3) was fitted to all data taken more than 450 feet from the source because the time constant correction is small and because this is the region of greatest concern to this particular method of aerial surveying. In table 1 the following data are given: column 1, the air distance in feet; column 2, the altitude in feet; column 3, the experimental counting rate; column 4, the counting rate multiplied by r/x; column 5, the data of column 4 divided by $\frac{e^{-\mu_0 r}}{r^2}[1+\mu_0 r-0.342(\mu_0 r)^2]$ yielding C; and column 6, the averages of column 5 with the nominal altitude and distance of the measurements offside.

The average values of C (table 1, column 6) are grouped so that any systematic deviation will point out an error made in the assumption of equation (3) for the elementary-source intensity. Within experimental error, the C's so obtained are equal. The observational error is calculated as the absolute mean deviation from the mean of data read by three observers from the same charts.

Using the values established for C and a_2, equations (3) and (4) become

$$I_p(x,\rho)=3.19\times 10^7 \frac{SA}{S_0 A_0}\frac{(x)}{r}\frac{e^{-\mu_0 r}}{r^2}[1+\mu_0 r-0.342\ (\mu_0 r)^2] \tag{6}$$

$$I_b(x)=3.19\times 10^7 2\pi \frac{S}{S_o A_o} e^{-\mu_o x}(1-0.342\mu_o x) \tag{7}$$

In figure 4, equation (6) at the point $r=x$ (directly overhead) is compared to experimental data corrected for the angle of view. The fit of the experimental data to the plot of equation (6) is particularly good for air distances less than 450 feet.

In figure 5, the intensity at different altitudes above an elementary source, calculated from equation (6), is plotted for flight lines directly over and at 125, 250, and 500 feet to the side of the source. It is clear that the maximum intensity increases with altitude as the distance of nearest approach to the flight lines is increased.

The accuracy of equation (7) in predicting the equivalent uranium content of broad sources can be determined by comparing it with the experimental equation (5) from which it follows that

$$3.19\times 10^7 \frac{2\pi S}{S_o A_o}=638, \text{ or } S=0.0018 \text{ percent } eU_3O_8 \tag{8}$$

The predicted value of 0.0018 percent equivalent U_3O_8 is considered a satisfactory fit with the analytical value of 0.0013 percent equivalent U_3O_8 for a large representative sample of the broad source.

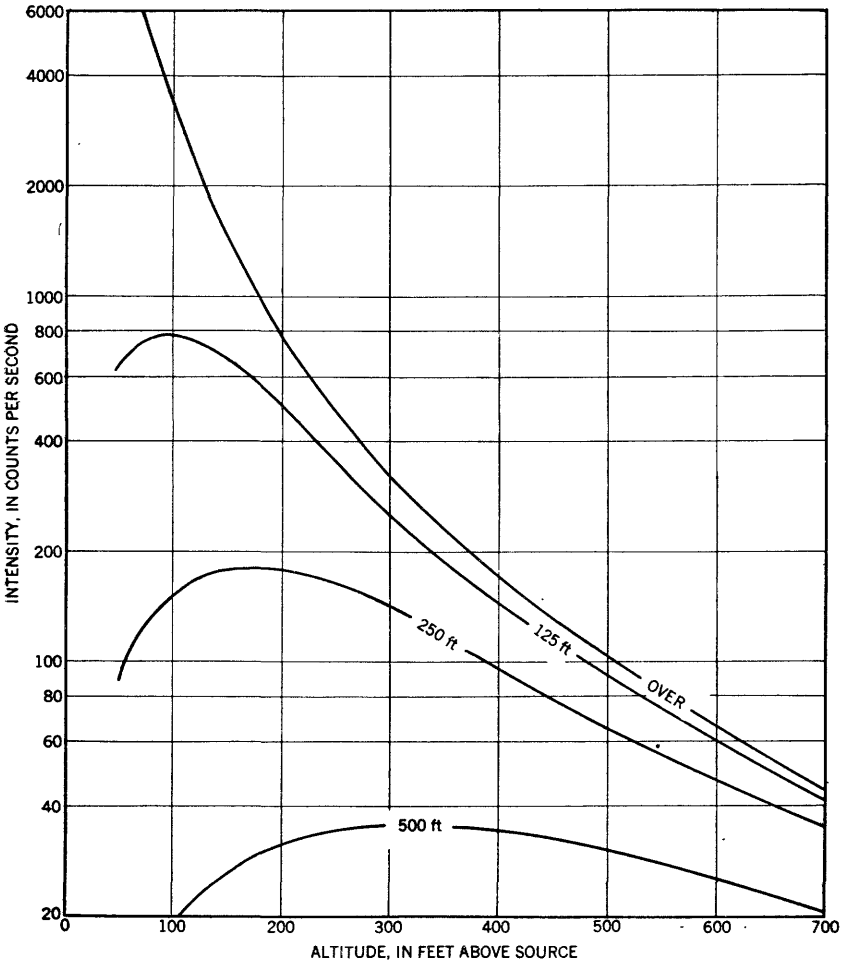

FIGURE 5.—Elementary-source intensity as function of altitude.

COMPARISON WITH THEORY

From existing computations of solutions to the Boltzmann equation in one medium and the knowledge of the primary spectrum of the uranium series, the expected integrated intensity from 0.4 Mev to 2.432 Mev was computed for the broad and elementary source of unit strength; that is, 1 photon per cubic foot per second and 1 photon per foot per second. The latter corresponds to a source 1 square foot in area emitting 1 photon per cubic foot per second. The details of the calculation are given on pages 37–38.

428734—57——3

For the purpose of this section, the following arbitrary nomenclature is adopted:

Primary intensity: Number flux due to unscattered photons from one line of the uranium series.

Total intensity: Number flux originating from a given line of the uranium series and including all energies degraded from that line down to 0.4 Mev, and including the unscattered flux. This is the response of a non-energy-dependent detector per square foot of detector area.

Primary flux: Superposition of all the primary intensities of the uranium spectrum above 0.4 Mev energy in proper proportion and normalized to unit source strength.

Total flux: Superposition of all the total intensities. This is the response of a nonenergy-dependent detector with a lower energy acceptance at 0.4 Mev. The cutoff has been chosen at 0.4 Mev as the spectrum of the uranium series is unambiguously known down to 0.34 Mev and as the Compton effect predominates in this range so that published one-medium computation can be adapted to two media.

Table 2, constructed from the work of Mladjenovic and Hedgran (1954) and Mladjenovic and Slatis (1954) and confirmed by Lazar (written communication, 1955), gives the energy of the gamma rays above 0.34 Mev and their fractional abundances. These are the values used in computing the individual intensities and the fluxes. Tables 3 and 4 contain the computed total and primary intensities and fluxes which are normalized to a broad source emitting 1 photon per cubic foot per second and are plotted in figures 6, 7, and 8.

In figure 6 the primary, scattered, and total intensities are plotted to an arbitrary scale for initial energies of 0.609 and 2.432 Mev, the two extremes in energy found in the spectrum. The importance of the scattered components, particularly for deeper penetrations, can be readily seen from the graph. The futility of any analysis in which scattering is neglected is obvious.

In figure 7, the computed total and primary fluxes are compared with the experimental data normalized to the theoretical value at the 500-foot altitude. The large deviation in slope between the curves labeled "data" and "primary" indicates the large contribution from degraded photons. The total flux and data agree well, even though the energy dependence of the detector has not been taken into account. The steeper slope of the computed curve relative to the experimental curve is to be expected because the computation weights all energies equally, whereas scintillation detectors are more efficient in detecting the low energies and both primary and scattered and the fractional contribution of primary flux to the total flux decreases with increasing distance from the source. Absolute agreement of computed with experimental data cannot be demonstrated because the true spectral efficiency of the detector is not known. However, one can compute the overall efficiency at 500 feet. Under the assumptions of 2 gamma

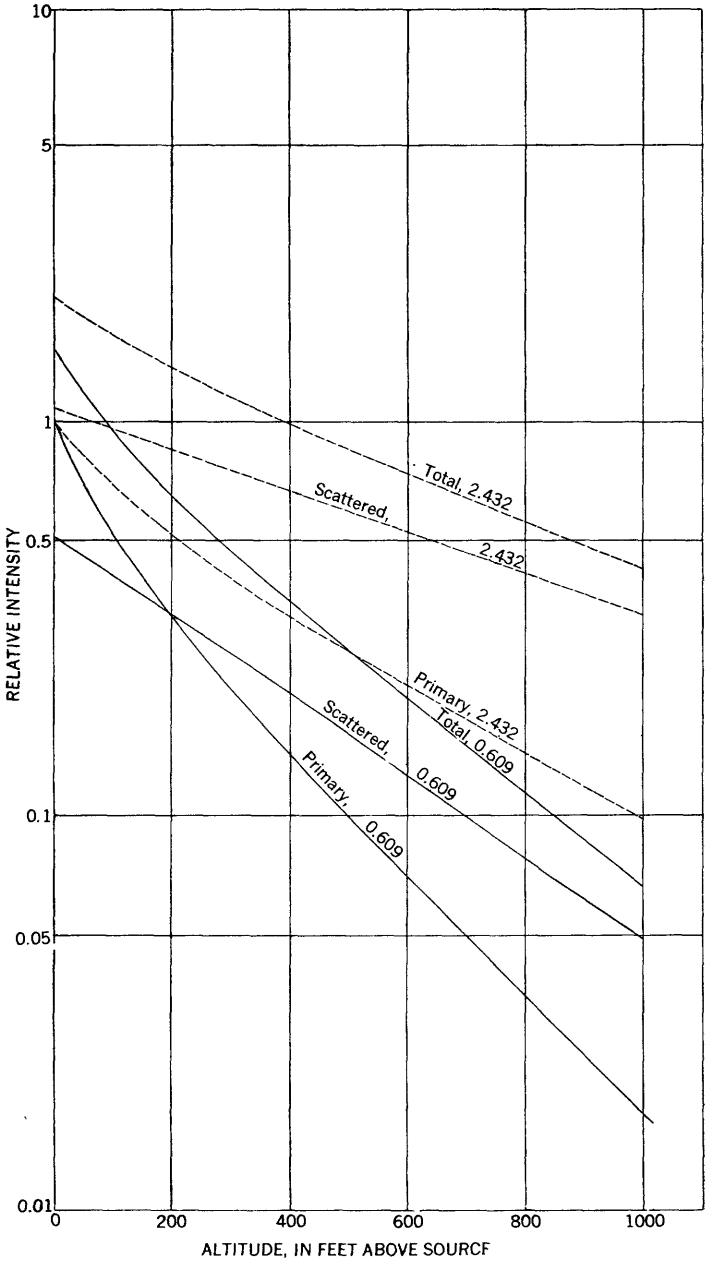

FIGURE 6.—Relative values of primary, scattered, and total intensities for primary energies of 2.432 and 0.609 Mev from broad source.

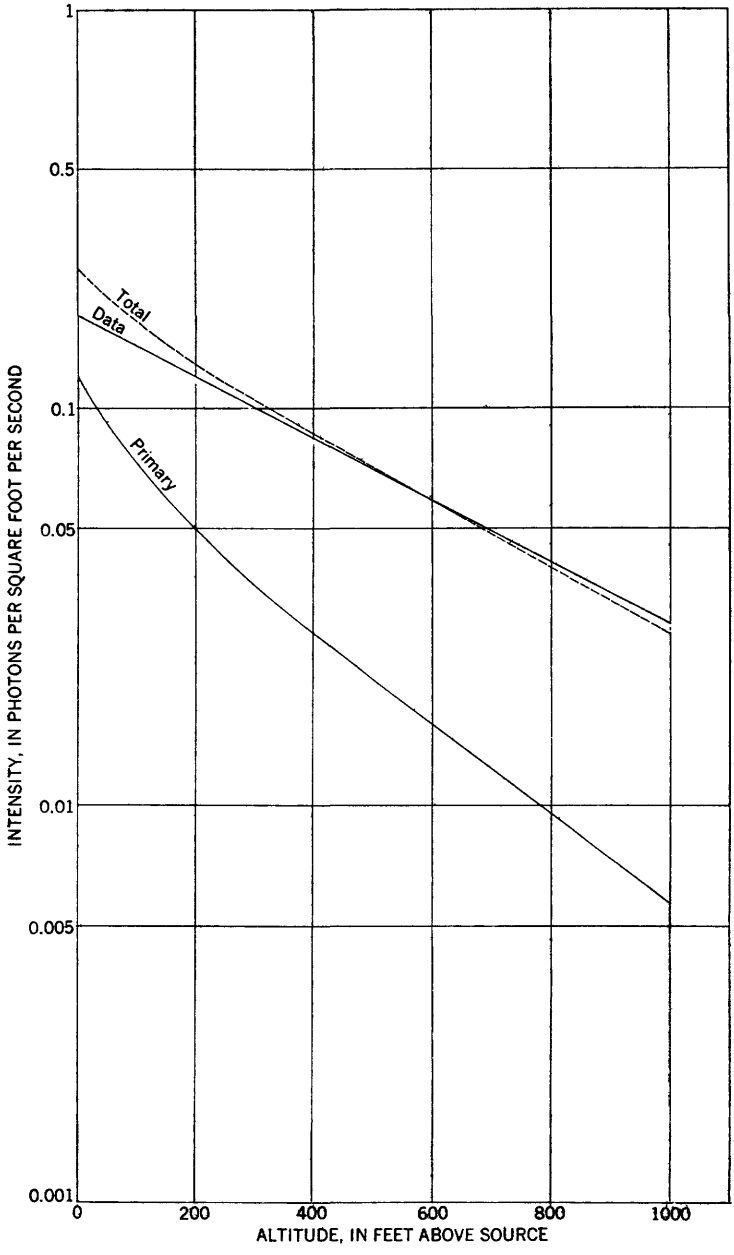

FIGURE 7.—Computed total and primary fluxes from broad source of uranium emitting 1 photon per ft² per second.

rays per disintegration of radium, a density of 2.3 for the source, a source concentration of 0.0013 percent eU_3O_8, and a detector area of 0.25 square feet, the expected counting rate is 597 counts per second for a 100 percent efficient detector. The experimental counting rate is 64 counts per second and the efficiency of the detector used is about 17 percent.

The decomposition of the flux and intensity from an elementary source of uranium are presented graphically in figures 8 through 11 in order to show the relative contribution of both primary and scattered radiation. The total primary flux (fig. 8) from a broad source is decomposed into the contributions from each of the primary energies given in table 2. For an elementary source, the calculated flux and intensities, normalized to the emission of 1 photon per foot per second, are given in tables 5 and 6 and plotted in figures 9, 10, and 11. The relative primary, scattered, and total intensities from 0.609 and 2.432 Mev primary gamma rays are presented in figure 9. The scattered intensity is again a significant proportion of the total intensity. A comparison of primary, total, and measured fluxes from an elementary source is given in figure 9, the source data being adjusted to agree with the computed total flux at 500 feet. The agreement in general behavior is excellent, the discrepancy being due to the equal weighting of energies in the computation. Finally, the decomposition of the total flux into contributions from each energy is shown in figure 11.

EFFECT OF TIME CONSTANT AND THE CONE OF RESPONSE

As computed on page 33–36, a continuously recording radiation detector in an aircraft flying at the 500-foot altitude at 220 feet per second directly over an elementary source will record 87 percent of the stationary value signal, whereas the same detector in an aircraft flying at the 100-foot altitude at 88 feet per second will record only 76 percent of the stationary value. The lag in recording the peak response at the 500- and 100-foot altitudes will be 0.320 and 0.675 of the time constant, respectively. Also, it may be seen from equation (6), on page 4, that for low-flying aircraft, a decrease in the product of velocity and time constant and (or) an increase in the cone of response will give an increased response. For high-flying aircraft the product of velocity and time constant should be made as low as possible.

GAMMA-RAY INTENSITY FROM IDEALIZED SOURCES AND INTERPRETATION OF RADIOACTIVITY ANOMALIES

On pages 3–11 semiempirical expressions of general validity were developed for the gamma-radiation intensities at considerable air distances from the two extreme types of natural thick uranium sources,

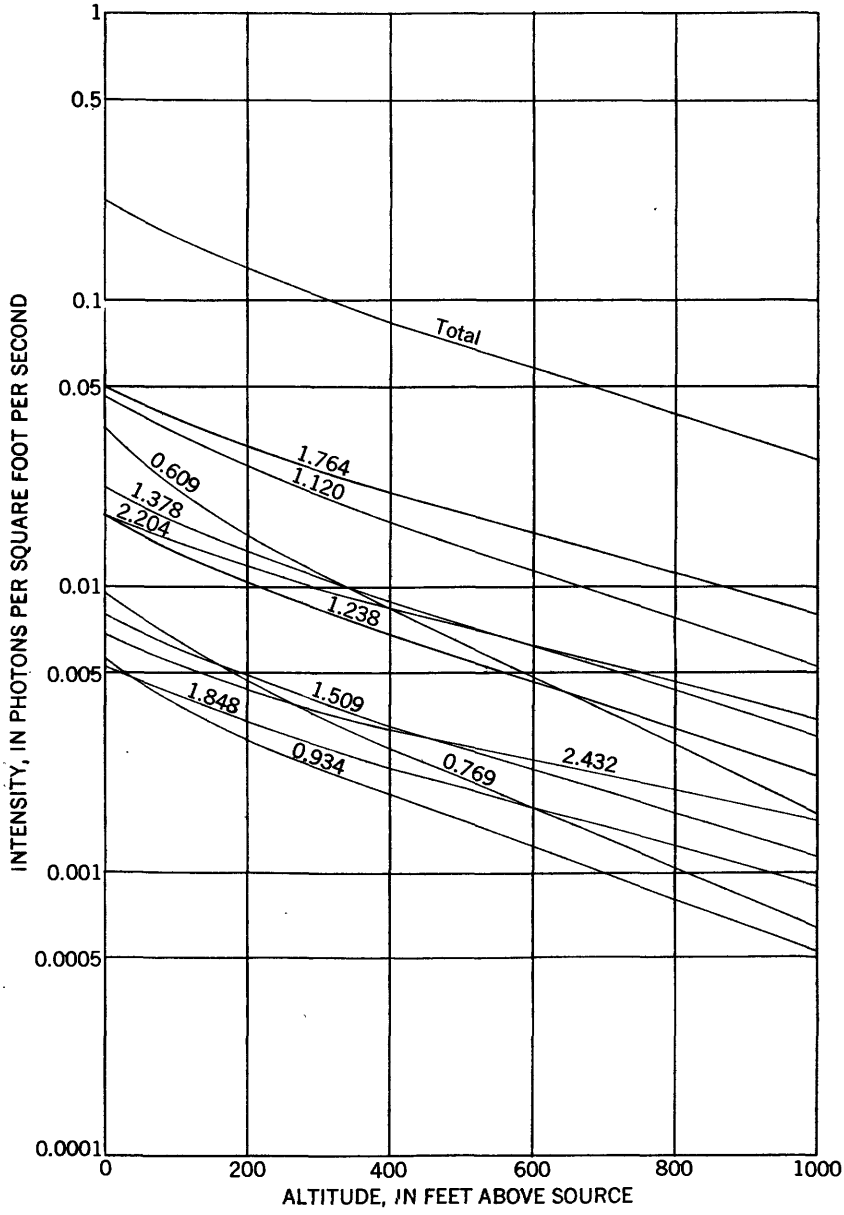

FIGURE 8.—Decomposition of total flux from broad source of uranium emitting 1 photon per ft² per sec. into contributions from several lines of spectrum.

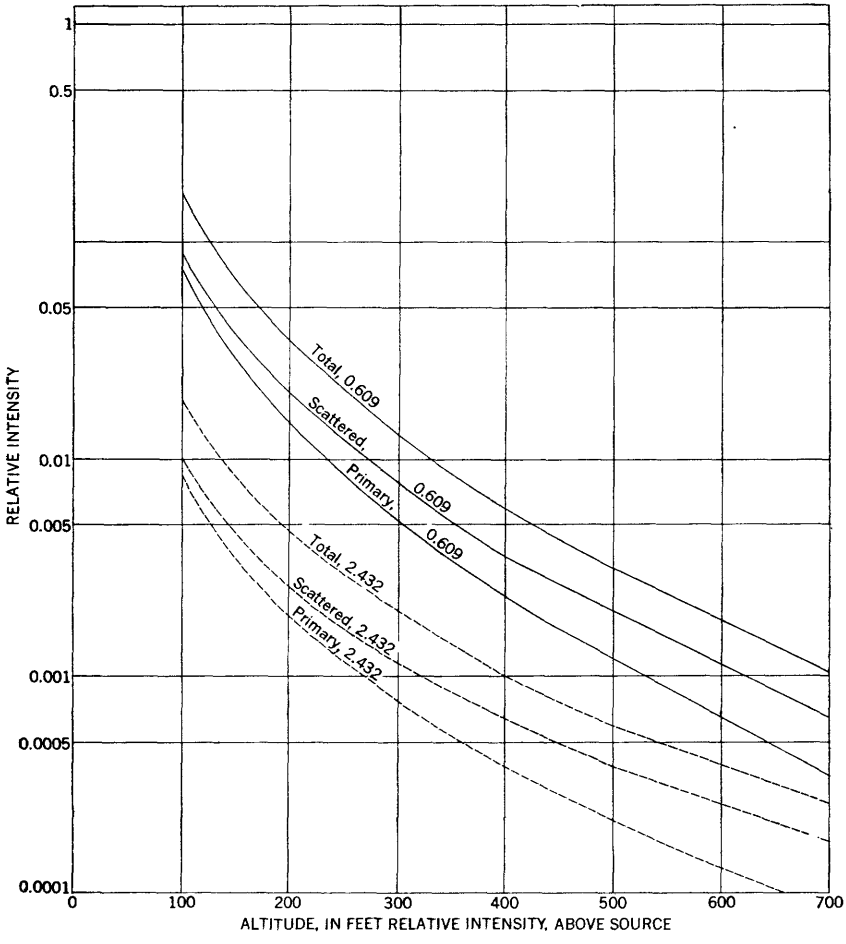

FIGURE 9.—Relative values of primary, scattered, and total intensities for primary energies of 2.432 and 0.609 Mev from elementary source.

the elementary and broad sources. To interpret semiquantitatively the measurements made in airborne radioactivity surveying, quantitative relationships must be established between the characteristics of natural sources intermediate between the two extremes of natural source types, and the observable quantities recorded by a specific detector of the counting-rate-meter type, such as the peak intensity, the area under the curve, and the shape of the curve.

In this portion of the report, the radiation intensity and area under the counting rate meter curve for idealized sources are established, their relation to the characteristics of the source is discussed, and a method of interpreting anomalies is given.

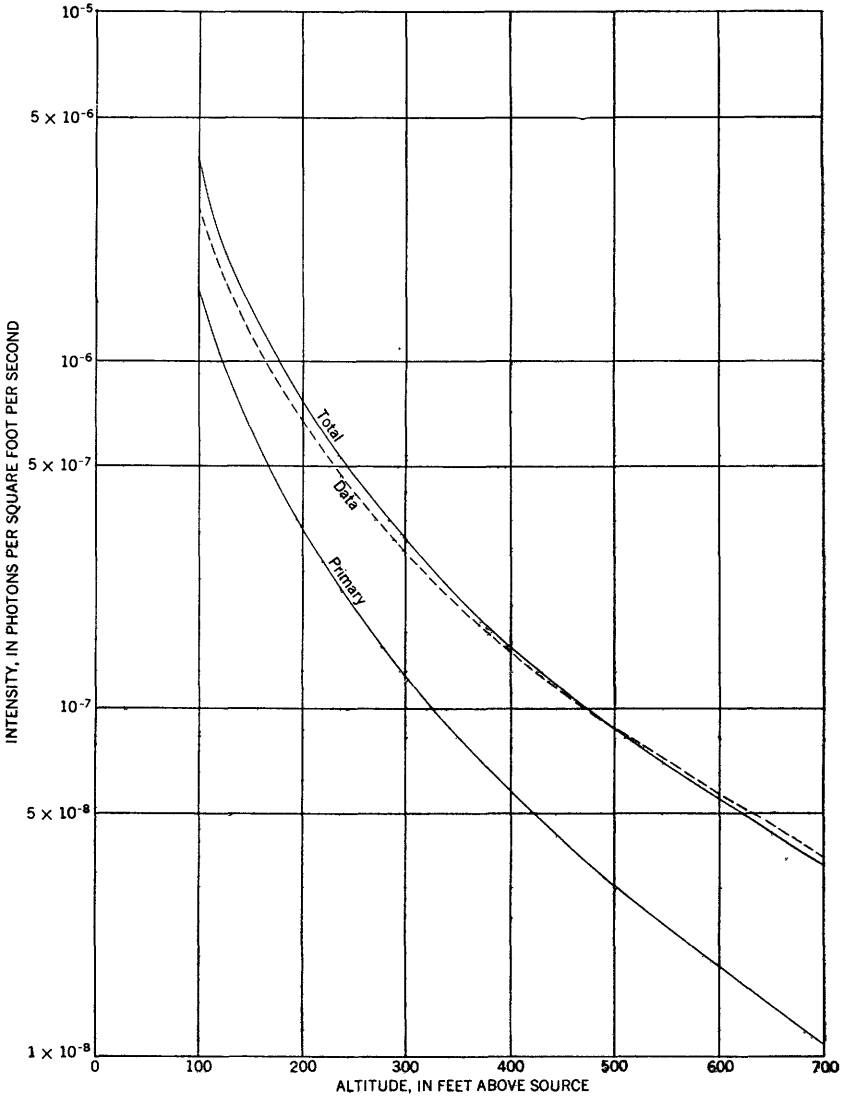

FIGURE 10.—Computed total and primary fluxes from elementary source of uranium emitting 1 photon per foot per second.

The unknown factors that enter into the interpretation of an anomaly are the source position relative to the detector, the surface dimension of the source, and the source strength in terms of equivalent uranium content. As the usual practice in airborne radioactivity surveying is to make continuously recorded measurements along equally spaced, constant-altitude flight lines, the location of an anomaly along the direction of flight can be determined with rela-

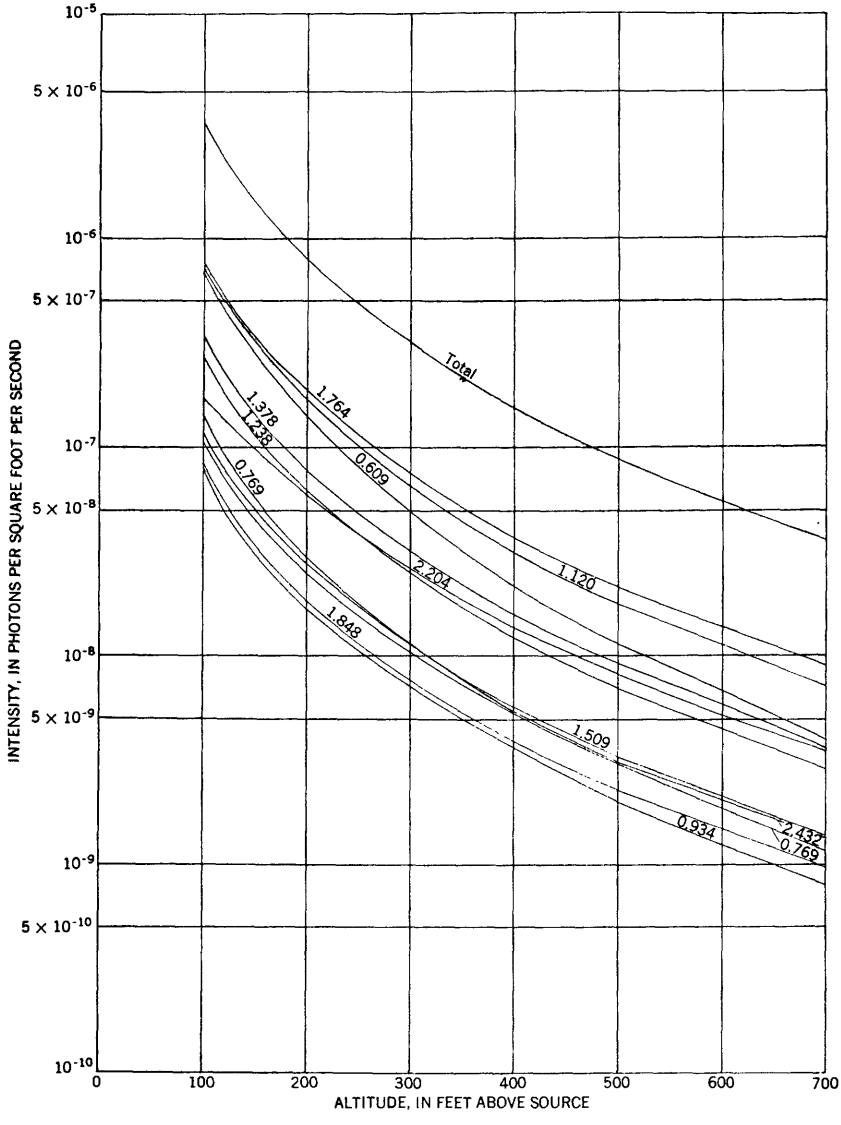

FIGURE 11.—Decomposition of total flux from elementary source of uranium emitting 1 photon per foot per second into contributions from several lines of spectrum.

tively small error. The location of an anomalous source is thus reduced to one unknown, the distance along the line normal to the flight path which passes through the peak position of the anomaly. If either linear or circular symmetry is assumed, the surface dimensions of the source are reduced to one variable, either the breadth of a slab source or the radius of a finite (circular) source.

428734—57——4

The three unknowns for any given source must be related to the observable data. The most obvious is the peak intensity; another is the area under the curve. A third is the shape of the curve, characterized by the slope or by the width at half-maximum intensity.

Computation of the peak intensities and areas under the curves for selected sources are made and criteria for distinguishing the different source types are established. Then the observable data are expressed directly in terms of source characteristics, eliminating explicit reference to the (unknown) distance between the source and the detector. Moreover, as natural sources vary greatly in grade, some grade-independent quantities readily computable from observable data should be used to determine salient characteristics of the sources.

SELECTED IDEALIZED SOURCES

The general behavior of the radiation intensities from natural sources is best discussed in terms of a few sources selected to approximate most nearly natural configurations. These sources are all assumed to be infinite in depth. Because of the absorption of radiation within the source, a thickness of 1 foot may be considered infinite.

Elementary source.—An elementary source is one whose areal extent is sufficiently small so that the radiation anomaly produced by it is identical to that produced by a theoretical point. The intensity, $I_p(x,\rho,a)$, from an elementary source (fig. 1, sec. *I*), is a function of x, the altitude of the detector above the source plane; ρ, the source-plane projection of the air distance between the source center and the detector; and a, the radius of the source. The area under the curve recorded by a count-rate meter, $H_p(x,z,a)$ is a function of previously defined x and a, and z, the source-plane projection of the air distance of nearest approach between the detector and source center.

Broad source.—A broad source is so large in areal extent that the intensities over the central region remain constant no matter how much additional source material is added to its boundary. The intensity, $I_b(x)$, from a broad source (fig. 2), is a function of x, the altitude above the source plane. The area under the curve is infinite.

Line source.—A line source is very large in length yet so narrow in width that the radiation anomaly produced by it is identical to that of a theoretical "line" source, one whose width is zero. The intensity, $I_l(x,y,a)$, from a line source which is infinite in length, is a function of x, the altitude of the detector above the source plane; y, the source-plane projection of the air distance from the detector to the source center line; and a, the width of the source. The area under

the curve recorded by a counting-rate meter, $H_l(x,\Theta,a)$ is a function of Θ, the angle between the flight line and the plane normal to the axis of the source, as well as of x and a. These variables are depicted in the insert to figure 14.

Slab source.—A slab source is so large in length that the radiation anomaly produced by it is a function of its width and independent of the length. The intensity, $I_s(x,y,a)$, and the area under the curve recorded by a counting-rate meter, $H_s(x,\Theta,a)$ are functions of the same variables as for the line source. The limiting value of the slab source as $a \rightarrow 0$ is the line source.

Finite source.—A finite source has a circular area of radius, a, which is intermediate in value to the elementary and broad source. The intensity, $I_f(x,\rho,a)$, and the area under the curve recorded by a counting-rate meter, $H_f(x,z,a)$, from a finite (circular) source of radius, a, are functions of the same variables as for the elementary source. The limiting case of the finite source as $a \rightarrow 0$ is the elementary source.

The above enumerated quantities are derived on pages 41–43. All numerical computations were performed under the assumption of quarter-mile flight-line spacing and a 500-foot flight altitude.

It is shown in equation (9), page 59 that for a particular flight level, the intensity of a finite source, I_f, is equal to a numerical constant times the function $G_3(x,\rho,a)$. The quantity $G_3(500,\rho,a)$ is tabulated in table 7 and plotted (fig. 12) for values of a against ρ. This plot of G_3 thus yields the relative intensities at several distances along a flight line at 500 feet above a finite source of fixed grade. The relative intensities plotted are equivalent to intensities that would be measured by a scintillation detector of short time constant in a plane flying at 500 feet above the ground along the flight line as shown in the insert to figure 12. The striking features are the rapid rise of the peak intensity with increasing radius of the source and slow increase in width of the anomaly with increasing radius. The minor variations in the slopes of the curves with major changes in radius militate against the determination of source size by slope analysis. The source 40 feet square by 6 inches thick at Grand Junction, Colo., used to establish the semiempirical equation for an elementary-source intensity, would give rise to too low an intensity to be depicted in this figure.

Similarly, it is shown in equation (8), page 42 that for a particular flight level, the intensity of a slab source, I_s, is equal to a numerical constant times the function $G_1(x,y,a)$. The quantity $G_1(500,y,a)$ is listed in table 8 and plotted in figure 13 for various values of a against y, yielding the relative intensities at various distances, y, along the flight line at 500 feet above slab sources of various sizes and of the

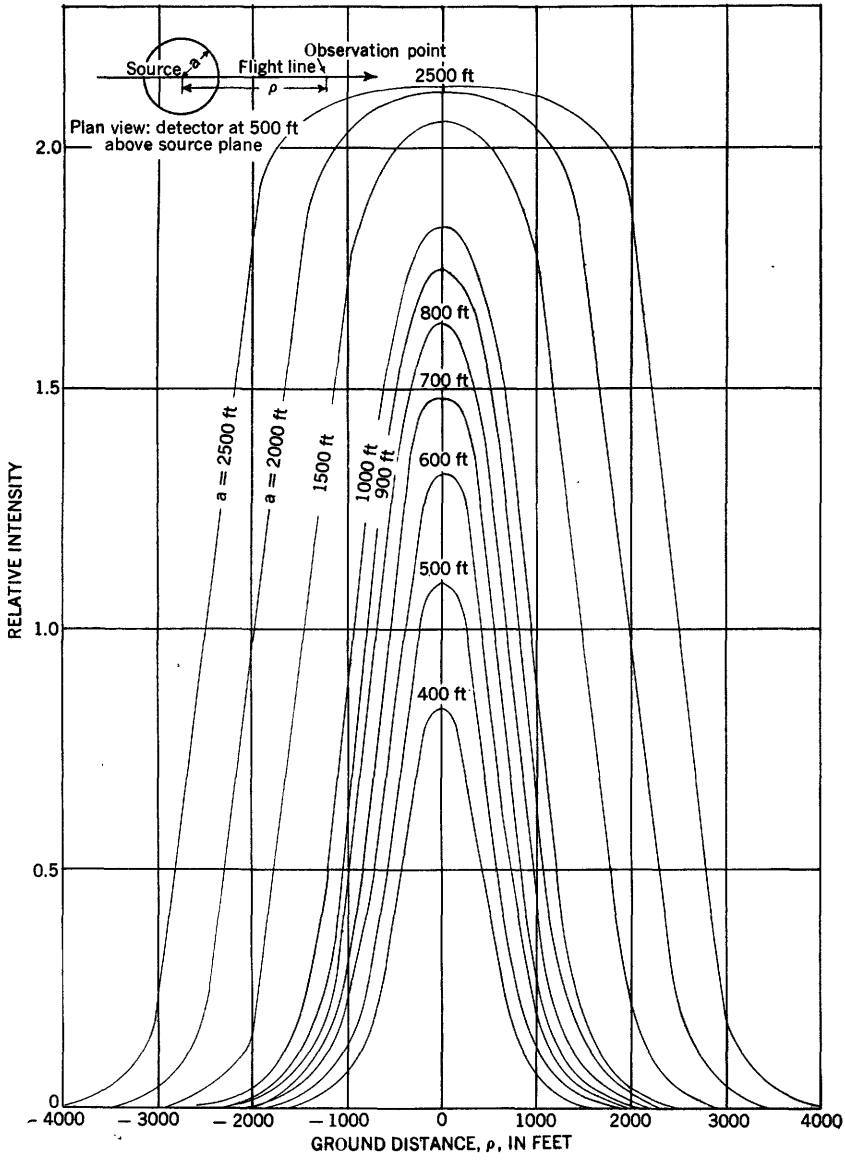

FIGURE 12.—Relative intensities at several distances from center of finite sources of several radii.

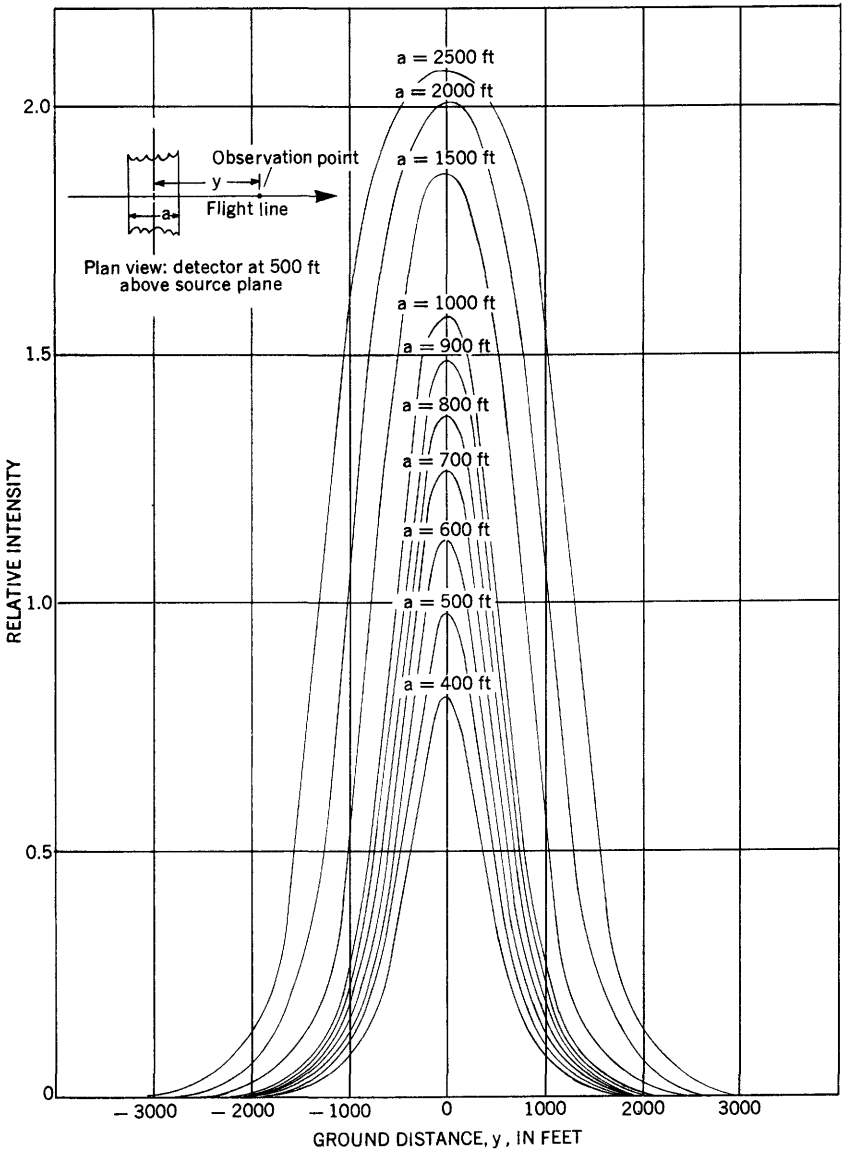

FIGURE 13.—Relative intensities at several distances from centerline of slab sources of several widths.

same grade. The curves are equivalent to profiles of anomalies that would be obtained under normal airborne surveying conditions. Again, slope analysis to determine source size is not feasible.

In figure 14, the relative intensities at 500 feet above a slab source 400 feet in width are plotted as a function of y', the ground projection of the air distance along the flight line from the detector to the center line of the source, where the individual curves are plotted for different angles of approach between the flight line and the center line of the source. The effect of oblique angles of approach completely invalidates any attempts at slope analysis.

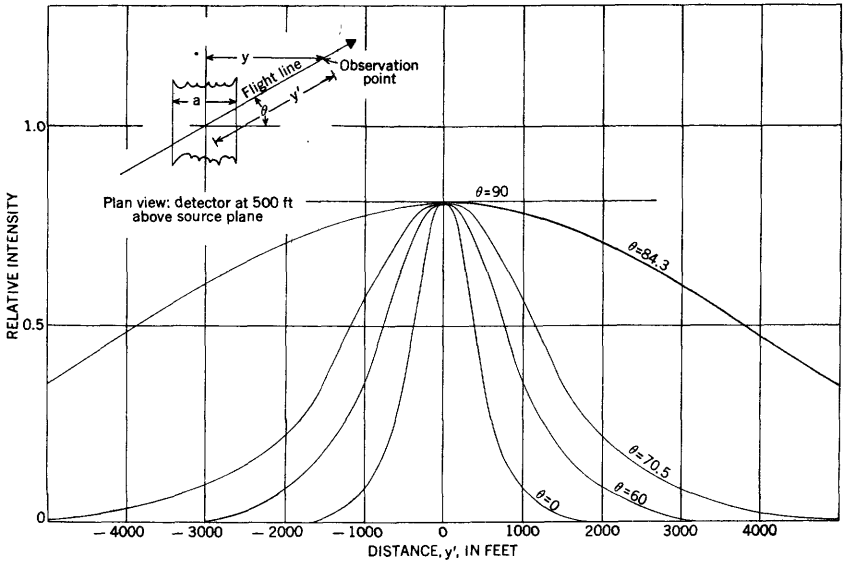

FIGURE 14.—Relative intensities at several distances from centerline of a slab source 400 feet wide at different angles of approach.

The impossibility of slope analysis is further illustrated in figure 15, where the relative intensities from finite sources of 400- and 500-foot radius are plotted against y, the distance along the flight line at 500 feet above the source plane, where the closest distance from the flight line to the source center is given by its ground projection, z, as shown in the insert. These curves can also be considered as identical with anomalies that would be actually recorded on these flight lines. The shapes are strongly dependent on the distance of the flight line from the source center.

Examination of figure 16 reveals another difficulty in utilizing the shape of anomalies to determine their sizes. One cannot, in general, say that the point where the intensity drops to a certain fraction of

the peak intensity is the edge of the source, for the intensity ratio at the edge to that of the center is one for zero radius (width) and asymptotically approaches one-half for an infinite radius (width). The limiting values are easy to understand: for zero radius (width), the edge and the center are the same point; whereas for the infinite radius (width), the point at the edge corresponds to slicing away exactly one-half of a broad source. Because of the rapid variation

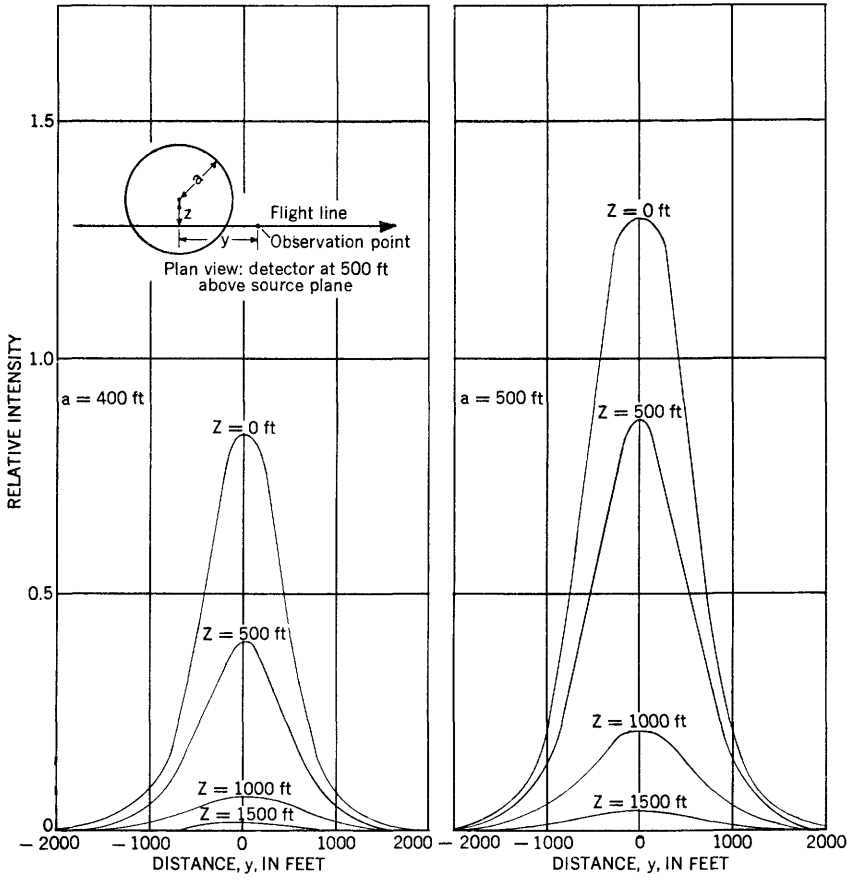

FIGURE 15.—Relative intensities at several distances along flight lines at different distances from center of finite sources of 400- and 500-foot radius.

of the ratio at small source dimensions, boundary identification by this method is impossible, but for broad sources, the one-half intensity point yields the source boundary.

In figure 17, curves *A* and *B* answer the question, "How infinite is infinity?" or what is the upper limit of the size of a finite or slab source required so that for a point centrally located 500 feet above the source, the intensity is essentially equivalent to that from an infinite broad

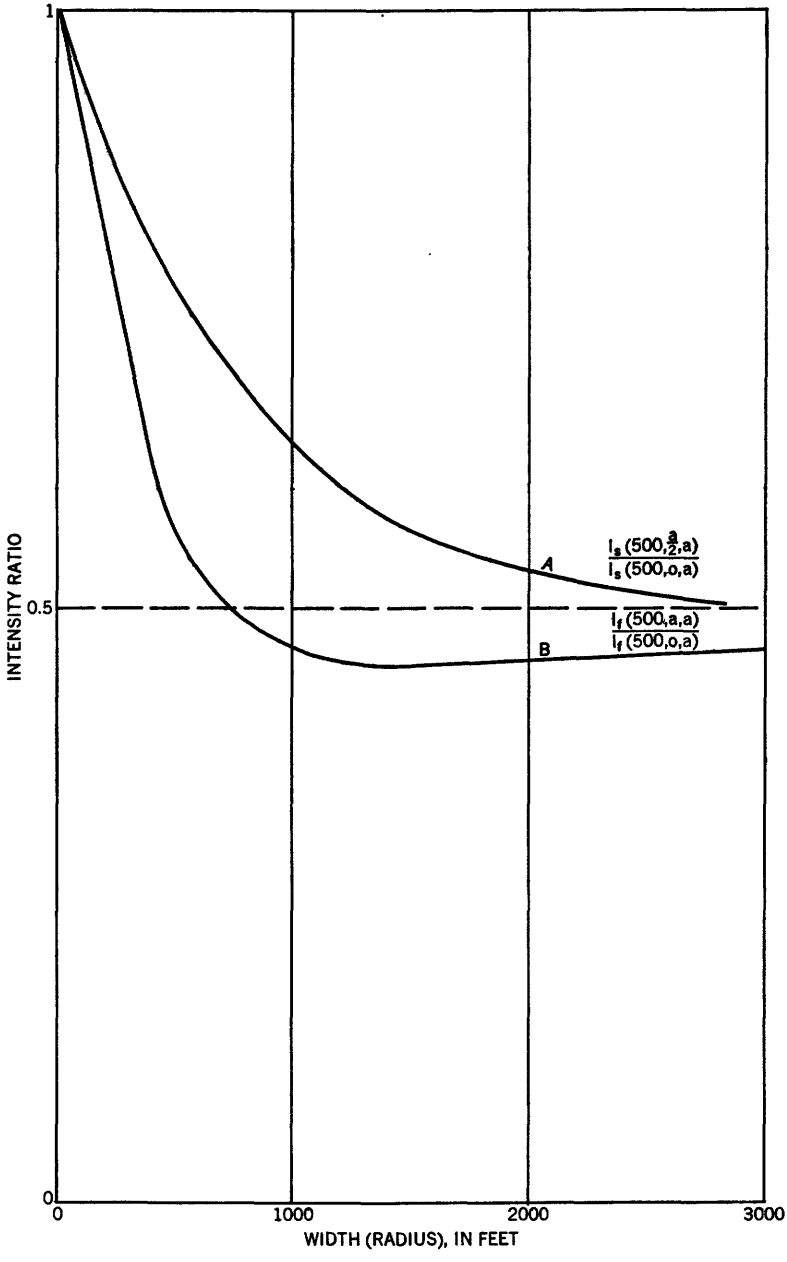

FIGURE 16.—Ratio of intensity at edge to intensity at center of source.

source. Curves A and B show (as a function of increasing radius or width) the ratio of the intensities from a finite and slab source respectively to the intensity of an infinite broad source. If it is assumed that for practical purposes 80 percent of the intensity from an infinite broad source would be indistinguishable from the intensity (or behavior) of an infinite broad source, then a finite or a slab source with a radius greater than 850 feet or a width greater than 1,200 feet respectively could be considered an infinite source. Curves A and B are

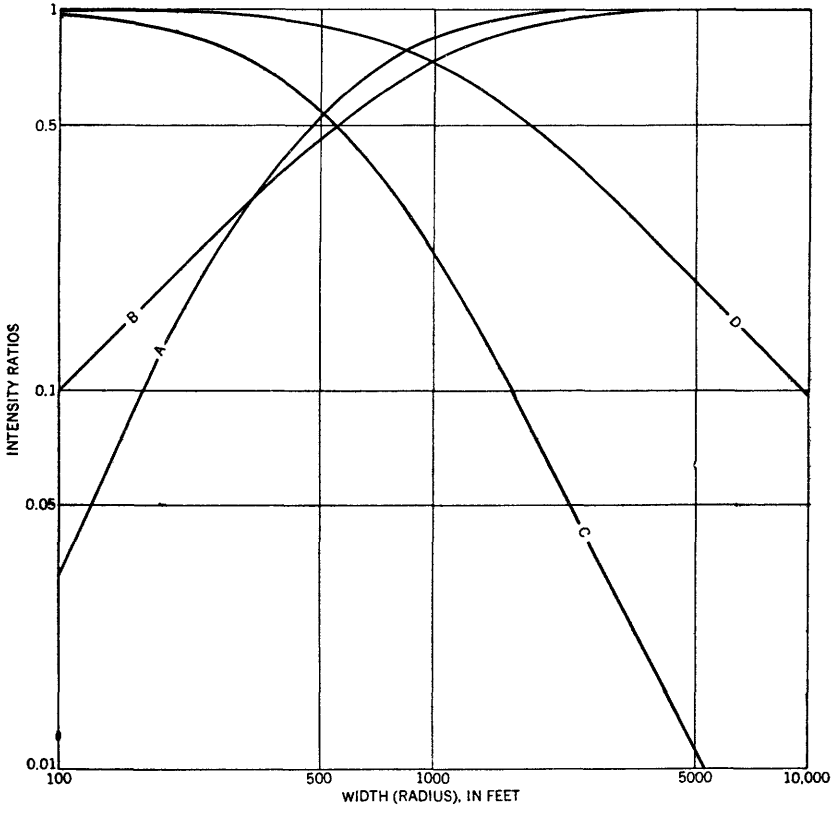

FIGURE 17.—Approach of intensity ratios to limiting value.

plots of expressions in equations (9) and (8) at ρ and y set equal to zero, both divided by expression in equation (2), where x in all cases is 500 feet (see equations (1), (8), (9), pages 41–42); thus, the curves are applicable only to measurements made at 500 feet above the source plane.

Curve C in figure 17 shows the ratio of the intensity from a finite source to that from an elementary source and thus indicates the lower limit of size of a finite source where the finite source intensity

would be essentially identical to that from an elementary source. If it is assumed for practical purposes that 80 percent of the intensity from an elementary source would be indistinguishable from the intensity (or behavior) of an elementary source, then a finite source with a radius less than 275 feet can be considered an elementary source. Curve C is a plot of expression in equation (9) divided by expression in equation (1), at ρ set equal to zero and x set at 500 feet (see equation (1) and (9), p. 41–42).

Curve D in figure 17 shows the ratio of the intensity from a slab source to that from a line source and indicates the lower limit of size where the slab source intensity would be essentially identical to that from a line source. If it is assumed for practical purposes that 80 percent of the intensity from a line source would be indistinguishable from the intensity (or behavior) of a line source, then a slab source with a width less than 800 feet can be considered a line source. Curve D is a plot of expression in equation (8) divided by expression in equation (4), where y is zero and x is 500 feet (see equations (4) and (8), p. 41–42).

For the specific radiation detection equipment currently used by the U. S. Geological Survey, the minimum detectable increase in counting rate is about 50 counts per second, equivalent to twice the standard deviation of measurement. Figure 18 shows the grade (eU_3O_8) of finite sources of radii that would be detectable at a 500-foot altitude of flight lines directly over, 600 feet away, and 1,300 feet away from the source center. Curve A gives the most unfavorable case in which the flight line is at a horizontal distance of 1,300 feet from the source center. Even then, an ore-grade body with more than 0.1 percent equivalent uranium and a minimum radius of 200 feet is detectable on two adjacent flight lines spaced at 1,300 feet (about ¼-mile) apart. Curves B and C are for the flight lines 600 and 0 feet away, and give correspondingly lower radii. Taking the 600-foot distance to be the most likely case, an ore grade body with a minimum radius of 600 feet located midway between flight lines spaced at 1,300 feet can be detected.

RELATIONSHIP OF OBSERVABLE DATA TO SOURCE CHARACTERISTICS

The general behavior of the radiation intensities from natural sources discussed above indicates that the useful observable quantities are the peak intensity I and the area under the curve H. The third readily apparent observable quantity, the shape of an anomaly as characterized by the slope or by the width at half-maximum intensity, has been demonstrated to be of little value for interpretation of source characteristics.

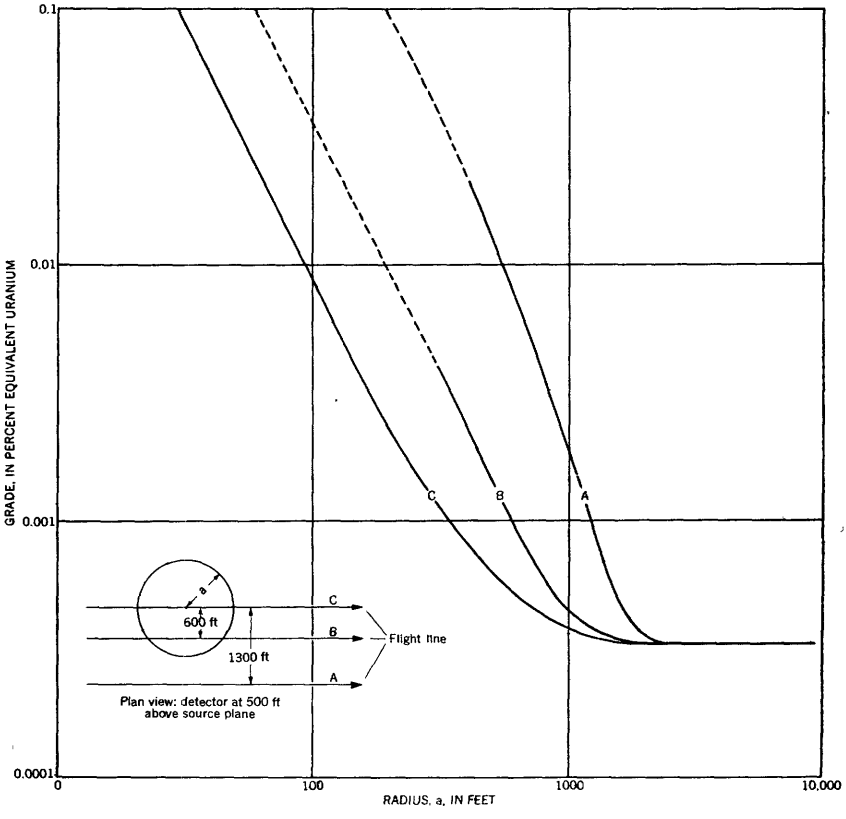

FIGURE 18.—Grade necessary to produce 50 counts per second for several radii of finite sources on different flight lines.

A plot (fig. 19) of $G_4(500,z,a)$ of table 9 against $G_3(500,z,a)$ of table 1 corresponds to a plot of arbitrarily scaled $H_f(500,z,a)$ against arbitrarily scaled $I_f(500,\rho,a)$ at the points where ρ equals z, the ground projection of the air distance of closest approach to the source center. This can be seen by dividing the expression in equation (9), (p. 42) by the expression in equation (7), (p. 43) to form $G_3/G_4=2I_f/H_f$. It is obvious that these plots are of little practical use as the scaling factors for real anomalies are unknown. However, by considering the graph, the following relationship is suggested.

$$G_4(500,z,a)=F(a)[G_3(500,z,a)]^{\alpha} \tag{1}$$

where $F(a)$ is a function of a. Now for the case of small a, the finite source reduces to an elementary source, and from equations (1) and (9), (p. 41–42) and equations (3) and (7) (p. 42–43), the functions $G_3(500,z,a)$ and $G_4(500,z,a)$ can be readily computed for small a.

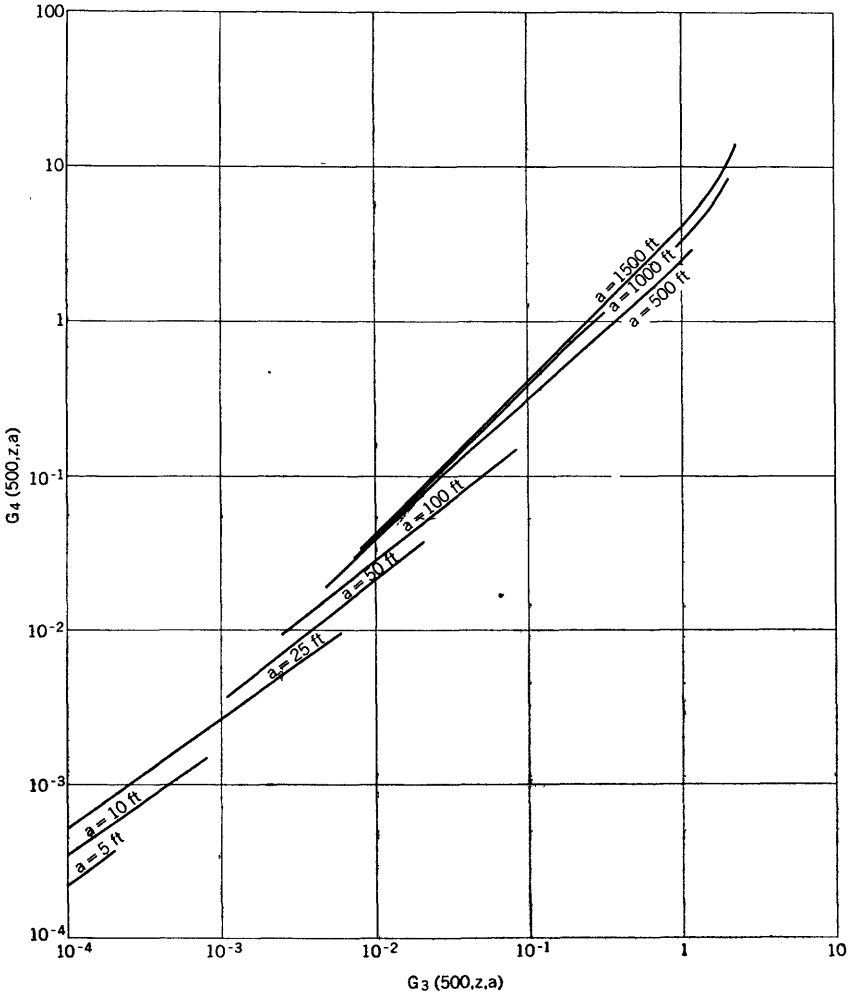

FIGURE 19.—Scaled area under curve $G_4(500,z,a)$ vs. scaled peak intensity $G_3(500,z,a)$ of finite sources of several radii (a).

Then, assuming the form of equation (1), and fitting the equation to the computed values, by the method of least squares, it is found that

$$G_4(500,z,a)\left(\frac{a}{500}\right)^{-2}\underset{a\to 0}{=}2.18\left[G_3(500,z,a)\left(\frac{a}{500}\right)^{-2}\right]^{0.788} \tag{2}$$

upon application of equations (9) (p. 42) and (7) (p. 43); the above equation becomes

$$\frac{H_f(500,z,a)}{\frac{4CS}{S_0A_0}(500\mu_0)\left(\frac{a}{500}\right)^2}\underset{a\to 0}{=}2.18\left[\frac{I_f(500,z,a)}{\left(\frac{a}{500}\right)^2\frac{2CS}{S_0A_0}500\mu_0}\right]^{0.788} \tag{3}$$

Thus, the grade-area, $S\pi a^2 = SA$,

$$SA = \left[\frac{S_0 A_0 500\pi}{2C\mu_0}\right]\left[\frac{4.36\{I_f(500,z,a)\}^{0.788}}{H_f(500,z,a)}\right]^{-\frac{1}{0.212}} \quad (4)$$

Thus, two transcendental equations, (9) (p. 42), and (7) (p. 43), in two unknowns, z and SA, were solved empirically to give explicit equation for grade-area for any value of z, in terms of the two observed quantities, $H_f(500,z,a)$ and $I_f(500,z,a)$. Equation (4) is true for elementary sources and approximately true for finite sources.

From tabulated values of $G_3(500, z, a)$ and $G_4(500, z, a)$ and from equations (9) (p. 42), and (7) (p. 43), insertion into equation (4) yields incorrect grade-area for a finite source. The ratio of this incorrect value to the true value of grade-area is listed in table 10, as a function of z and a. One notes that the range in values is considerable. However, for any fixed a, the arithmetic mean of the grade-area ratios calculated at z and at .1300–z (average of ratios over two flight lines straddling the source center) is reasonably constant as shown in table 11. The arithmetic mean at a fixed radius of the reciprocals of the values in table 6 is taken, and these average values are listed in table 12 along with maximum and minimum values of the reciprocals at a fixed a. Thus, if the approximate surface dimension of the source were known, application of equation (4) followed by multiplication by the proper correction factor in table 12 should yield the correct grade-area of finite sources. The tabulated extreme values in table 12 indicates that the error in source location entails only 15 percent error in the correction factor.

It remains now to determine the radius of the finite source. A useful grade independent quantity is $\frac{H_f(500,z,a)}{I_f(500,z,a)}$ which is tabulated in table 13. In figure 20, the data in table 13 at z is plotted against the quantity at 1300–z for values of a, a comparison of data from two adjacent flight lines straddling the source. The solid curve represents a given source radius; the dotted curves connect constant ground distances from the nearer flight line to the source z. To get grade-area, one can get the radius of the source and closest distance of approach from this plot and apply a correction from the proper entry in table 10 to the computed value from equation (4). However, a 10 percent error in H and I would result in an error of the ratio K/I, represented by the grid length in figure 20. This could result in a possible error in z by as much as 600 feet and an error in a by 200 feet. The variation with distance, z, of predicted to true grade-area ratios at a given radius is quite serious, as an examination of table 10 will show. Thus, it is better to estimate by figure 20 what

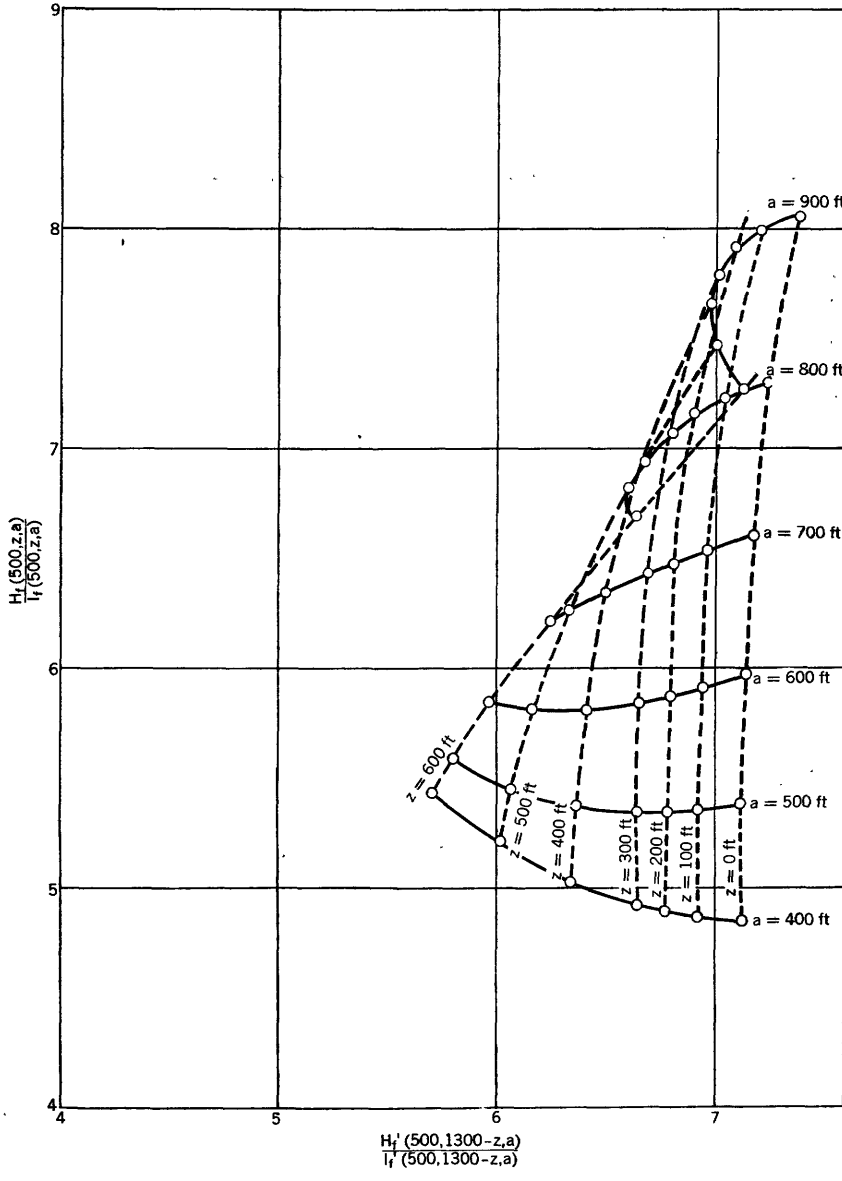

FIGURE 20.—Ratio of area under curve (H_f) to peak intensity (I_f) at z vs. ratio of area under curve (H_f' to peak intensity (I_f') at 1300-z for finite source of several radii.

the radius is, to compute the grade-area on two adjoining lines through equation (4), and to apply the proper correction factor in table 12. With grade-area and radius known, it would be easy to find the grade.

For slab sources table 14 furnishes the quantity, $\frac{H_s(500,o,a)}{I_s(500,o,a)}$ which is plotted in figure 21 as function of the slab width, a. These grade-independent quantities can be used to estimate the width of the slab source. Once the width is determined, the grade can be determined from equation (8) (p. 42) with y set equal to zero.

INTERPRETATION OF ANOMALIES

Based on the foregoing discussions, the following method suggests itself. H and I represent respectively the measured area under a curve recorded on a counting rate-meter and the peak intensity reading. The procedure would be:

1. *If the anomaly shows distinctive flattening at the peak.*—The source can then be considered a broad source, and the grade computed from equation (2) (p. 41). The boundary of the source is at the one-half peak intensity point.

2. *If the anomaly is visible on one flight line.*—As an ore-grade body greater than 200 feet in radius would be visible on two lines and as any finite source of radius smaller than 275 feet can be considered an elementary source, application of equation (4) p. 41, yields the grade-area.

3. *If the anomaly is visible on two lines.*—Two cases are possible, namely:

a. If the anomalies on two adjacent lines are approximately equal, it is a slab source. Compute $H_s(500,o,a)$ from the relation, $H_s(500,o,z)=H\cos\Theta$. The angle, Θ, is determined from the relative displacement of the peaks on the two adjacent lines. Then from figure 21 and from the computed $H_s(500,o,a)/I$, determine a. From equation (8), p. 42, with y set equal to zero and the measured I, determine grade-width and thence, the grade.

b. If the anomalies are not equal in amplitude, it is a finite source. Let subscripts 1 and 2 denote two adjacent flight lines with the highest peaks, and $I_1>I_2$. Then with H_1/I_1 as ordinate and H_2/I_2 as abscissa, determine a from figure 20. Compute SA on lines 1 and 2 and average the results. Multiply the average by the factor in table 12 corresponding to the proper a. The result is the grade-area from which grade can be obtained.

CONCLUSIONS

Comparison of experimental data with theoretical calculation shows fair agreement for both the broad and the elementary sources, outside a multiplicative constant. Thus, the effect of the interface

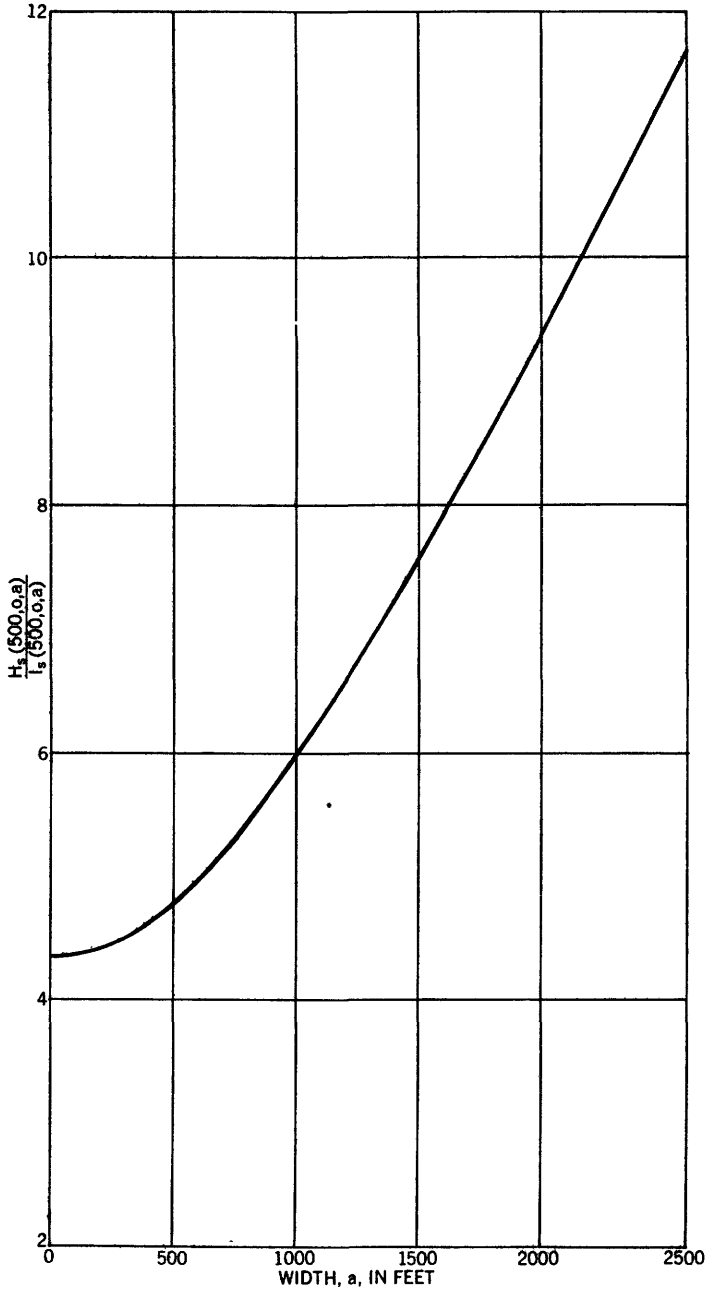

FIGURE 21.—Ratio of area under curve (H_s) to peak intensity (I_s) vs. width of a slab source at $\theta=0$.

and the effect of the spectral energy responses of different detectors can be approximately taken into account by merely changing a multiplicative constant. This result can be attributed to the fact that radiation emerging from thick sources possesses an equilibrium spectrum that does not change appreciably in traversing a mean free path of air.

It should be pointed out that the data of tables 3 and 4 can be adjusted for altitudes above sea level other than that at Grand Junction, Colo., by using the appropriate μ, a function of air density, to correct tabulated values for different air distances from the source. The values in tables 5 and 6 can be similarly adjusted after multiplying by x^2 because in this case $r=x$. The density of the source was taken to be 2.3; for other densities, corrections should be applied inversely as the densities.

Certain general concepts underlying the semiempirical approach to airborne radioactivity surveying warrant attention. These are:

1. Use of an elementary source of finite thickness instead of the classical point source. In calculating the intensity of a theoretical point source at an interface, it is necessary to take into account scattering and absorption and the effect of the interface. This requirement is circumvented by observing the radiation intensity from an elementary source of infinite thickness, because the measurements themselves already contain the effects of both scattering and absorption and of the interface.

2. Use of the form and structure predicted by theory for the analytical expressions of the intensities to insure that correction for conditions differing from the ones prevailing during experimental measurements can be made unambiguously.

3. Use of elementary- and broad-source data to determine the constants in the elementary-source intensity expression.

4. The investigation, numerically and analytically, of the relationship between particular observable quantities and characteristics of sources selected to approximate natural sources.

The two observable quantities useful for determining grade-area relationship are the peak intensity and the area under the curve. The shape of the anomaly such as the breadth or slope at half-maximum intensity, cannot be used for interpreting grade-area and (or) grade of natural sources although shape is useful in determining source type.

This particular method of utilizing the peak intensity and the area under the curve, for the interpretation of natural source characteristics is not unique. For example, once the source types have been identified the grade might be computed on the assumptions that the source

is either directly below the detector or at the point midway between two adjacent flight lines, yielding the two extreme values of grade.

Based on investigation, numerical and analytical, of the relationship among the observable quantities and natural source characteristics, the following sequence is established for interpretation of actual anomalies:

1. Identification of one of five source types—the elementary, the finite, the slab, the line, and the broad source—by appearance of an anomaly, either on one or on two or more adjacent flight lines, by the relative magnitudes of the anomaly on adjacent flight lines, or by flattening of the peak of the anomaly.
2. Use of grade-independent observable quantities to determine source size.
3. Determination of grade (grade-area and grade-breadth) of sources without reference to the (unknown) distance from source to detector.

The following results have been established for the conditions of surveying used by the U. S. Geological Survey.

1. Broad sources are finite sources that are greater than 850 feet in radius and slab sources that are greater than 1,200 feet in width.
2. Elementary sources are finite sources less than 275 feet in radius.
3. Line sources are slab sources less than 800 feet in width.
4. Line and slab sources greater than 1,700 feet in length are infinite in length.

In application of equation (4), the total fractional error in the determination of the grade-area, $\frac{\partial(SA)}{SA}$, is related to the errors in H and I by

$$\left|\frac{\partial(SA)}{SA}\right| \leqq 4.73\frac{\partial H}{H}+3.73\,\frac{\partial I}{I}=8.5b$$

where b is the fractional error in measurement assumed to be the same for both H and I. Thus, in order to obtain the grade-area within a factor of two, the error in measurement must be less than 12 percent. Moreover, to obtain the grade within a factor of two, the sum of the fractional error in grade-area and twice the fractional error in a must be less than 1. Particularly, in the case of overlapping anomalies, the uncertainty of resolving a compound anomaly into component anomalies will introduce very large errors in both H and I for the component anomalies.

The method of interpretation of the grade of broad sources is highly accurate as shown by many field investigations (R. M. Mox-

ham, oral communication). Interpretation of the grade-width and grade of slab or line sources is also satisfactory. Finite and elementary sources, particularly those visible on only one flight line, are difficult to interpret; insufficient data are available to evaluate the accuracy of interpretation.

COMPUTATION OF INTENSITIES

The computed values (Goldstein and Wilkins, 1954) are the quantities $4\pi r^2 I_0(\mu_i r, E, E_i)$ where $I_0(\mu_i r, E, E_i)$ are the scattered energy flux at energy, E, distance, r, from the source, originating from a point source of energy E_i and strength 1 photon per second, for several media. μ_i is the linear attenuation coefficient. Of the various media in Goldstein's tabulation, air is most nearly approximated by the Compton scatterer.

The quantity

$$B(\mu_i r, E_i) = \int_{0.4}^{E_i} 4\pi r^2 I_0(\mu_i r, E, E_i) \frac{dE}{E} \tag{1}$$

was computed for energies $E_i = 0.5$, 1.0, 2.0, 3.0, and 4.0 Mev, and $\mu_i r = 1$, 2, 7, 10, 15, and 20. The trapezoidal rule was used except at the end points where linear interpolation was followed by direct integration of the interpolant. Then quadratic interpolation was performed over these to find $B(\mu_i r, E_i)$ for the 11 primary energies of the uranium series. The result was 77 values of $B(\mu_i r, E_i)$.

As the solution of multi-media Boltzmann equation of pure Compton scatterer in one distance variable can be cast into one-medium form, an exact solution can be obtained for the broad source by computing as though the media were homogeneous

$$I_b(x, E_i) = \int_0^{\cos^{-1} x/r} \int_y^{\infty} \frac{e^{-\mu_i r}}{4\pi r^2} B(\mu_i r, E_i) 2\pi r^2 \, dr \sin\Theta \, d\Theta \tag{2}$$

$$= \frac{e^{-\mu_i{}^s y}}{2\mu_i{}^s} \int_0^{\infty} \frac{u}{u + \mu_i{}^s y} B(u + \mu_i{}^s y, E_i) e^{-u} \, du$$

$$= \frac{e^{-\mu_i{}^a x}}{2u_i{}^s} \int_0^{\infty} \frac{\mu}{u + \mu_i{}^a x} B(u + \mu_i{}^a x, E_i) e^{-u} \, du$$

$$\mu_i{}^s y \equiv \mu_i{}^a x$$

For the case of an elementary source, such an equality does not exist, and we assume that the two-media elementary-source expression is given as $\frac{1}{r^2} f(\mu_i{}^s (r - x) + \mu_i{}^a x)$ wherein the scattered intensity at point x directly over head is

$$I_p(x,E_i)=\int_x^\infty \frac{e^{-\mu_i^s(r-x)-\mu_i^a x}}{4\pi r^2}\,dr\,B(\mu_i^s(r-x)+\mu_i^a x)$$

$$=\frac{e^{-\mu_i^a x}}{4\pi}\,\mu_i^s\int_0^\infty \frac{e^{-u}}{(\mu+\mu_i^a x)^2}\,B(u+\mu_i^a x,E_i)\,du \qquad (3)$$

which is not exact. The integrations in either case are performed by the method of Gauss wherein

$$\int_0^\infty f(x)e^{-x}\,dx\sim\sum_{k=1}^{n_i}\left[\frac{dL_n(x)}{dx}\right]^{-2}_{x=x_k} f(x_k) \qquad (4)$$

where $L_n(x_k)=0$, x_k's being the n roots of Laguerre Polynomial of order n.

Thus

$$I_b(x,E_i)\sim\frac{e^{-\mu_i^a x}}{2\mu_i^s}\sum_{k=1}^{5}\left[\frac{1}{\dfrac{dL_5(x)}{dx}}\right]^2_{x=x_k} B(x_k+\mu_i^a x,E_i)\,\frac{x_k}{x_k+\mu_i^a x} \qquad (5)$$

$$I_p(x,E_i)\sim\frac{e^{-\mu_i^a x}}{4\pi}\,\mu_i^s\sum_{k=1}^{5}\frac{\left[\dfrac{dL_5(x)}{dx}\right]^{-2}_{x=x_k}}{(x_k+\mu_i^a x)^2}\,B(x_k+\mu_i^a x,E_i) \qquad (6)$$

The B's were plotted on log-log papers and read off the graph for 5 values of the argument for each x point and energy value.

The primary intensity expressions can be readily found.

$$I_b^0(x,E_i)=\frac{1}{2\mu_i^s}\int_1^\infty \frac{e^{-\mu_i^a xy}}{y^2}\,dy \qquad (7)$$

$$I_p(x,E_i)=\frac{1}{4\pi}\frac{e^{-\mu_i^a x}}{\mu_i^s}\left[e^{+\mu_i^s x}\int_1^\infty \frac{e^{-\mu_i^s xy}}{y^2}\,dy\right]\sim\frac{1}{4\pi\mu_s^i}\,\frac{e^{-\mu_i^a x}}{x^2} \qquad (8)$$

Equations (7) and (8) multiplied by the relative abundance of table 2 are listed in tables 4 and 6 under their respective energy headings for several values of x. The final column is the sum of all these components.

The sum of equations (7) and (5) and the sum of equations (6) and (8) multiplied by the relative abundances are found in tables 3 and 5 under respective energy headings. The final column again represents the sum.

The superscripts a and s refer to air and source respectively.

CALCULATION OF DETECTOR RESPONSE

The relative response of a counting-rate meter at time t to a elementary source of intensity I is

$$R(t)=\int_{t_0}^t e^{-(t-t')}\,I(t')dt' \qquad (1)$$

where time is expressed in units of the time constant, T, of the instrument, t_0 is the time the source first falls within the cone of response of the detector, and the origin of time is chosen as the moment of closest approach. Expansion about $t=0$ exists for this integral, i. e.,

$$R(t)=\sum_{m=0}^{\infty}\left.\frac{d^nR(t)}{dt^n}\right|_{t=0}\frac{t^n}{n!} \tag{2}$$

where the derivatives satisfy the relationship

$$\frac{d^nR(t)}{dt^n}=-\frac{d^{n-1}R(t)}{dt^{n-1}}+\frac{d^{n-1}I(t)}{dt^{n-1}}\Bigg]_{t=0} \tag{3}$$

$$R(O)=\int_0^{t_0}e^{-y}f(z)\,dt' \tag{4}$$

$$y=t'+z \qquad z^2=x^2+z^2+\beta^2t'^2=r^2+\beta^2t^2$$

where:

x=altitude in mean free paths
z=ground projection of distance of closest approach
β=distance traveled in one time constant in mean free paths
$t_o=\dfrac{x^2\tan^2\alpha-z^2}{\beta}$
α=½ angle of the cone of response

By partial integration

$$R(O)\sim\frac{-e^{-y}f(z)}{\frac{dy}{dt'}}-\frac{e^{-y}}{\left(\frac{dy}{dt'}\right)}\frac{d}{dt'}\left(\frac{f(z)}{\frac{dy}{dt'}}\right)\Bigg]_o^{t_o} \tag{5}$$

Because the result of the partial integration is a semi-convergent series, within the range of parameters pertinent to airborne surveying the minimum error is incurred by evaluating only the first term at the upper limit, and both terms at the lower limit:

$$R(o)\sim e^{-r}f(r)\left\{(1-\tilde{\omega})-\frac{\beta^2}{r}\right\} \tag{6}$$

where

$$\tilde{\omega}=\frac{e^{-z_0}f(z_0)e^{-t_0}}{\left[1+\beta^2\frac{t_0}{z_0}\right]e^{-r}f(r)}$$

$$z_0=x\sec\alpha$$

Then the ratio of the response to the stationary value at the point of closest approach is

$$\frac{R(t)}{e^{-r}f(r)}=\sum_{n=0}^{\infty}\frac{A_nt^n}{n!} \tag{7}$$

where

$$A_0=1-\omega-\frac{\beta^2}{r} \tag{8}$$

$$A_1=\tilde{\omega}+\frac{\beta^2}{r} \tag{9}$$

$$A_2=-\tilde{\omega}-\frac{\beta^2}{r} \tag{10}$$

$$A_3=\tilde{\omega}+\frac{f'(r)}{f(r)}\frac{\beta^2}{r} \tag{11}$$

$$A_4=-\left(\tilde{\varphi}+\frac{f'(r)}{f(r)}\frac{\beta^2}{r}\right) \tag{12}$$

The maximum is found from the equation

$$\sum_{n=1}^{\infty}\frac{A_n\, t^{n-1}}{(n-1)!}=0 \tag{13}$$

If we retain only two terms, we find

$$t_2=1 \tag{14}$$

the same result as found by Peirson (1951). If we retain three terms

$$t_3=\frac{-A_2+\sqrt{A_2^2-2A_1\,A_3}}{2} \tag{15}$$

If we retain four terms, we can expand the cubic about t_3 to a linear term and find

$$\frac{t_4}{t_3}\sim 1-\frac{A_4}{A_2+A_3}\frac{t_3}{3!} \tag{16}$$

Then the insertion of t_4 into equation (7) yields the ratio of peak response to the stationary value. This is carried out for

$\alpha=45°$, $z=0$, and	$\tau=1$ second for two typical cases:
$x=0.730$ (500 feet)	$x=0.146$ (100 feet)
$\beta=0.329$ (220 fps)	$\beta=0.128$ (88 fps velocity)
$t_2=1$	$t_2=1$
$t_3=0.323$	$t_3=0.635$
$t_4=0.320$	$t_4=0.675$
$\frac{R(t_4)}{e^{-x}f(x)}=0.873$	$\frac{R(t_4)}{e^{-x}f(x)}=0.76$

It should be noted that due to the nature of the approximation the result can be considered the lower limit of the peak response. To recapitulate, the ratio of peak response to stationary value is

$$\frac{R(t)}{e^{-\tau}f(r)}\sim\left(1-\tilde{\omega}-\frac{\beta^2}{r}\right)+\left(\tilde{\omega}+\frac{\beta^2}{r}\right)t-\left(\tilde{\omega}+\frac{\beta^2}{r}\right)\frac{t^2}{2!}+\left(\tilde{\omega}+\frac{\beta^2}{r}\frac{f'(r)}{f(r)}\right)\frac{t^3}{3!}-\left(\tilde{\omega}+\frac{\beta^2}{r}\frac{f'(r)}{f(r)}\right)\frac{t^4}{4!} \quad (17)$$

where

$$\frac{t}{t_3}=1-\frac{\tilde{\omega}+\frac{\beta^2}{r}\frac{f'(r)}{f(r)}}{1-\frac{\beta^2}{r}\frac{f'(r)}{f(r)}}\frac{t_3}{3!} \quad (18)$$

$$t_3=\frac{\left(\tilde{\omega}+\frac{\beta^2}{r}\right)+\sqrt{\left(\tilde{\omega}+\frac{\beta^2}{r}\right)^2-2\left(\tilde{\omega}+\frac{\beta^2}{r}\right)\left(\tilde{\omega}+\frac{\beta^2}{r}\frac{f'(r)}{f(r)}\right)}}{2}$$

INTENSITY FROM SELECTED SOURCES

It was shown previously in equation (6), p. 10 that the intensity from an elementary source is

$$I_p(x,\rho,a)=\frac{CSA}{S_0A_0}\frac{x}{r^3}e^{-\mu_0 r}(1+\mu_0 r-\gamma(\mu_0 r)^2)=\frac{CSA}{S_0A_0}xf_1(r) \quad (1)$$

where

S=source grade in percent eU
S_0=source grade in percent eU standard=0.35 percent
A=area of source=πa^2
A_0=Area of standard source=1600 ft.^{2}
$r^2=x^2+\rho^2$
$\mu_0=1.461\times10^{-3}$ ft.$^{-1}$ at sea level
$\gamma=0.342$
$C=3.19\times10^7$

and from a broad source is

$$I_b(x)=\frac{2\pi CS}{S_0A_0}e^{-\mu_0 x}(1-\gamma\mu_0 x) \quad (2)$$

we rewrite

$$f_1(r)=\sqrt{\frac{2}{\pi r}}\int_{\mu_0}^{\infty}pK_{1/2}(pr)\,p^{1/2}\,dp-\gamma\mu_0{}^2\sqrt{\frac{2\mu_0}{\pi r}}K_{1/2}(\mu_0 r) \quad (3)$$

where $K_{1/2}$ is modified Bessel function of the second kind, order 1/2. The line source intensity is

$$I_l(x,y,a)=\frac{CS}{S_0A_0}a\,x\int_{-\infty}^{\infty}dz\,f(R)=\frac{2\,CS}{S_0A_0}axf_2(\omega) \quad (4)$$

where

$R^2=x^2+y^2+z^2$
$\omega^2=x^2+y^2$

It is known (Watson 1948) that

$$\int_0^\infty K_\nu \left[p\sqrt{t^2+z^2}\right] \left[t^2+z^2\right]^{-\frac{z}{2}} dz = \sqrt{\frac{\pi}{2p}}\, K_{\nu-\frac{1}{2}}(pt)\, t^{\frac{1}{2}-z} \tag{5}$$

$$\therefore f_2(\omega) = \int_0^\infty f_1(R)\, dz = \int_{\mu_0}^\infty p\, K_0(p\omega)\, dp - \mu_0 K_0(\mu_0\omega) = \mu_0^2 \left[\frac{K_1(\mu_0\omega)}{(\mu_0\omega)} - K_0(\mu_0\omega)\right] \tag{6}$$

$$\therefore I_l(x,y,a) = \frac{2CS}{S_0 A_0}\, \mu_0^2\, ax \left[\frac{K_1(\mu_0\omega)}{\mu_0\omega} - \gamma K_0(\mu_0\omega)\right] \tag{7}$$

The slab source intensity is

$$I_s(x,y,) = \frac{2\,CS}{S_0 A_0}\, \mu_0^2 x \int_{-a/2}^{a/2} \left[\frac{K_1(\mu_0 R)}{\mu_0 R} - \gamma K_0(\mu_0 R)\right] dz = \frac{2\,CS}{S_0 A_0} \mu_0 x\, G_1(x,y,a) \tag{8}$$

where

$$R^2 = x^2 + (y-z)^2.$$

$G_1(500,y,a)$ is tabulated in table 8.

The finite source intensity is

$$I_f(x,\rho,a) = \frac{2\,CS}{S_0 A_0}\, x \int_0^\pi d\zeta \int_0^a y\, dy = \frac{2\,CS}{S_0 A_0}\, \mu_0 x\, G_3(x,\rho,a) \tag{9}$$

where

$$R^2 = x^2 + \rho^2 - 2\rho y \cos\zeta + y^2$$

$G_3(500,\rho,a)$ is tabulated in table 7.

AREA UNDER COUNTING-RATE-METER CURVE

The response, $R(t)$, of a counting-rate meter of response time at time t to a time dependent signal $I(t)$ is

$$R(t) = \frac{1}{\tau}\int_{-\infty}^{t} e^{-\frac{(t-t')}{\tau}}\, I(t')dt' \tag{1}$$

Then the area under curve, H, is

$$H \equiv \int_{-\infty}^{+\infty} R(t)dt = \int_{-\infty}^{\infty} I(t')dt' \tag{2}$$

For the elementary source

$$H_v(x,z,a) = \int_{-\infty}^{\infty} I_v\left(x,\sqrt{z^2+v^2t^2},a\right) dt \tag{3}$$

$$= \frac{2CSA}{S_0 A_0}\, x \int_0^\infty f_1(R)\, dt'$$

$$= \frac{2CSA}{S_0 A_0} \left(\frac{\mu_0^2 x}{v}\right) \left[\frac{K_1(\mu_0 s)}{\mu_0 s} - \gamma K_0(\mu_0 s)\right]$$

where $s^2=x^2+z^2$ and v is the velocity of the detector.
For the line source

$$H_l(x,\theta,a)=\int_{-\infty}^{\infty} I_l(z, vt'\cos\theta, a)\,dt'=\frac{4CS}{S_0A_0}\,\mu_0^2\,ax\int_0^{\infty}\left[\frac{K_1(\mu_0 R)}{\mu_0 R}-\gamma K_0(\mu_0 R)\right]dt' \tag{4}$$

where $R^2=x^2+v^2t^2\cos^2\Theta$. Thus,

$$H_l(x,\theta,a)=\frac{2\pi CS}{S_0A_0}\left(\frac{a}{v\cos\theta}\right)e^{-\mu_0 x}(l-\gamma\mu_0 x)=\frac{4CS}{S_0A_0}(\mu_0 x)\,G_2(x,\theta,a) \tag{5}$$

For the slab source

$$H_s(x,\theta,a)=\int_{-\infty}^{+\infty} I_s(x, vt'\cos\theta, a)\,dt'=\frac{4CS}{S_0A_0}(\mu_0 x)\,G_2(x,\theta,a) \tag{6}$$

identical to the line source.

For the finite source

$$H_f(x,z,a)=\int_{-\infty}^{+\infty} I_f(x,\sqrt{z^2+v^2t'^2},a)\,dt'=\frac{4CS}{S_0A_0}(\mu_0 x)\,G_4(x,z,a) \tag{7}$$

The function $G_4(500,z,a)$ is tabulated in table 9.

LITERATURE CITED

Cook, J. C., 1952, An analysis of airborne surveying for surface radioactivity: Geophysics, v. 17, no. 3, p. 607–706.

Fano, U., 1953a, Penetration of X- and gamma-rays to extremely great depth: U. S. Nat. Bur. Standards Jour. Research, v. 51, no. 2, p. 95–121.

——— 1953b, Gamma-ray attenuation: Nucleonics, v. 11, no. 8, p. 8–12; no. 9, p. 55–61.

Goldstein, Herbert and Wilkins, J. Ernest, 1954, Calculations of the penetration of gamma-rays, final report: U. S. Atomic Energy Comm. NYO–3075, issued by U. S. Atomic Energy Comm. Tech. Inf. Service, Oak Ridge, Tenn.

Mladjenovic, M. and Hedgran, Arne, 1954, An investigation of the Compton secondaries from RaC gamma rays: Arkiv för Fysik, Band. 8, Hafte 4, p. 49–63.

Mladjenovic, M. and Slatis, H., 1954, Internal conversion spectrum of the active deposit of radon: Arkiv för Fysik, Band 8, Hafte 4, p. 65–82.

Peirson, D. H. and Franklin, E., 1951, Aerial prospecting for radioactive minerals: British Jour. Applied Physics, v. 2, p. 281–291.

Spencer, L. V. and Fano, U., 1951, Penetration and diffusion of X-rays. Calculation of spatial distribution by polynomial expansion: U. S. Natl. Bur. Standards Jour. Research, v. 46, no. 2, p. 446–456.

Stead, F. W., 1956, Instruments and techniques for measuring radioactivity in the field, *in* Page, L. R, Stocking, H. E., Smith, H. B., (compilers), Contributions to the geology of uranium and thorium by the United States Geological Survey and Atomic Energy Commission * * *, p. 705–713.

Steljes, F., Cowper, G., and Carmichael, H., 1952, Aerial prospecting for radioactive material: Canada Natl. Research Council, Rept. no. CRR–495.

Watson, G. N., 1948, A treatise on the theory of Bessel functions: 2d ed., Cambridge University Press, 417 p.

TABLE 1.—*Elementary-source data and associated computations*

Air distance r (feet)	Altitude x (feet)	Experimental intensity (counts per second)	Experimental intensity $\times\left(\frac{r}{x}\right)$	C	C (average)
600 feet nominal altitude, 375 feet offside					
560	470	45±5	53.6±6.0	2.21×10^7	$(2.57\pm0.42)\times10^7$
626	530	42.5±2.5	50.2±3.0	2.74	
583	510	40	45.8	2.09	
601.3	520	57.5±12.5	66.5±14.5	3.27	
500 feet nominal altitude, 375 feet offside					
526	405	60	77.9	2.748	$(3.36\pm0.70)\times10^7$
605	440	55±5	75.6±6.9	3.768	
566	440	55±5	70.8±6.4	2.996	
552	420	90	118	4.696	
581	455	45±5	57.4±6.4	2.584	
400 feet nominal altitude, 375 feet offside					
485	315	45±5	69.3±7.7		
462	300	82.5±2.5	127 ±4		
480	315	65±5	99 ±7.6		
455	320	70	99.6		
471	285	87.5±2.5	145 ±4		
600 feet nominal altitude, 250 feet offside					
580	540	70 ±10	75.2	3.38	
622	570	30	32.8	1.76	$(3.40\pm0.70)\times10^7$
619	580	77.5±7.5	82.6±10.6	4.35	
577	520	67.5±2.5	74.9± 2.8	3.32	
586	530	82.5±2.5	91.2± 2.8	4.20	
500 feet nominal altitude, 250 feet offside					
543	490	62.5±2.5	69.3±2.8	2.650	
485	425	60	68.4	1.987	$(2.59\pm0.34)\times10^7$
516	480	65±5	69.8±5.4	2.34	
472	415	103±3	117 ±3	3.18	
465	415	95±5	106 ±6	2.80	
400 feet nominal altitude, 250 feet offside					
364	285	148±3	189 ±3		
402	315	125±5	160 ±6		
364	285	106±5	134 ±6		
387	320	125±5	151 ±6		
389	315	103±3	127 ±9		
600 feet nominal altitude, 125 feet offside					
472	465	120	122	3.32	
476	470	130	132	3.66	$(3.09\pm0.10)\times10^7$
449	445	120	121	2.94	
442	440	143	143		
506	500	83±3	83.4±2.4		
490	490	87.5±2.5	87.5±2.5	2.61	
500 feet nominal altitude, 125 feet offside					
405	395	173±3	177 ±3		
416	410	123±18	124 ±18		
417	415	145±5	146 ±5		
453	445	100	102		
430	425	130	132		

TABLE 1.—*Elementary-source data and associated computations*—Continued

Air distance r (feet)	Altitude x (feet)	Experimental intensity (counts per second)	Experimental intensity $\times\left(\frac{r}{x}\right)$	C	C (average)
400 feet nominal altitude, 125 feet offside					
327	320	143±43	146±43	----------	----------
311	300	273±3	283	----------	----------
332	325	180	184	----------	----------
285	275	350	363	----------	----------
336	325	203±8	209±8	----------	----------
600 feet nominal altitude, 0 feet offside					
473	470	155±6	156±6	4.27	----------
486	485	175±20	175±20	5.135	----------
515	515	100±7	100±7	3.37	$(4.14\pm0.53)\times10^7$
550	550	110±10	110±10	4.34	----------
536	535	96.7±8.9	96.9±8.9	3.58	
500 feet nominal altitude, 0 feet offside					
470	470	133±9	133±9	----------	----------
461	460	140±7	140±7	----------	----------
460	460	148±2	148±2	----------	----------
460	460	118±8	118±8	----------	----------
446	445	163±2	164±2	----------	----------
400 feet nominal altitude, 0 feet offside					
325	325	272±6	272±6	----------	----------
310	310	310±7	310±7	----------	----------
325	325	282±6	282±6	----------	----------
320	320	255±3	255±3	----------	----------
290	290	332±8	332±8	----------	----------
300 feet nominal altitude, 0 feet offside					
260	260	427±6	427±6	----------	----------
260	260	437±6	437±6	----------	----------
260	260	433±10	433±10	----------	----------
260	260	460±7	460±7	----------	----------
245	245	490±7	491±7	----------	----------
200 feet nominal altitude, 0 feet offside					
140	140	1400	1400	----------	----------
140	140	1480	1480	----------	----------
160	160	1350	1350	----------	----------
145	145	1620	1620	----------	----------
145	145	1550	1550	----------	----------
100 feet nominal altitude, 0 feet offside					
111	110	2810±260	2840±260	----------	----------
86	85	3930±10	3990±10	----------	----------
87	85	3650	3730	----------	----------
85	85	4000	4020	----------	----------
85	85	3940±10	3960±10	----------	----------

TABLE 2.—*Primary gamma rays of uranium series*

Energy (Mev)	Abundance	Energy (Mev)	Abundance
0.609	0.268	1.509	0.0292
.769	.0579	1.764	.164
.934	.0282	1.848	.0172
1.120	.204	2.204	.0522
1.238	.0741	2.432	.0188
1.378	.0869		

TABLE 3.—*Total flux and total intensities of various components from uranium broad source emitting 1 photon per foot³ per second*

Altitude (feet)	Energy (Mev)											Total flux (photons per ft² per sec)
	0.609	0.769	0.934	1.120	1.238	1.378	1.509	1.764	1.843	2.204	2.432	
	Total intensity (photons per square foot per second)											
0	0.0362	0.00967	0.00561	0.0469	0.0182	0.0226	0.00809	0.0497	0.00531	0.0183	0.00692	0.228
100	.0222	.00643	.00389	.0337	.0131	.0166	.00607	.0377	.00406	.0141	.00545	.163
200	.0155	.00469	.00293	.0263	.0104	.0134	.00482	.0308	.00341	.0117	.00455	.130
300	.0133	.00357	.00237	.0212	.00830	.0108	.00397	.0256	.00277	.00987	.00385	.106
400	.00831	.00273	.00188	.0170	.00678	.00893	.00327	.0215	.00230	.00840	.00329	.0844
500	.00624	.00212	.00151	.0138	.00552	.00741	.00270	.0182	.00198	.00720	.00284	.0695
600	.00472	.00169	.00122	.0113	.00459	.00610	.00227	.0154	.00168	.00606	.00246	.0575
700	.00359	.00132	.000987	.00865	.00380	.00512	.00194	.0131	.00143	.00527	.00211	.0473
800	.00266	.00104	.000801	.00818	.00311	.00420	.00161	.0110	.00122	.00455	.00186	.0402
900	.00211	.000764	.000651	.00626	.00259	.00359	.00133	.00895	.00104	.00396	.00161	.0329
1,000	.00158	.000654	.000525	.00518	.00215	.00299	.00114	.0081	.000889	.00342	.00141	.0280

TABLE 4.—*Primary flux and primary intensities of various components from uranium broad source emitting 1 photon per foot³ per second*

Altitude (feet)	Energy (Mev)											Primary flux (photons per ft² per sec)
	0.609	0.769	0.934	1.120	1.238	1.378	1.509	1.764	1.848	2.204	2.432	
	Primary intensity (photons per square foot per second)											
0	0.0239	0.00573	0.00305	0.0243	0.00926	0.0114	0.00406	0.0246	0.00263	0.00877	0.00333	0.121
100	.0123	.00310	.00174	.0142	.00553	.00700	.00252	.0158	.00170	.00579	.00226	.0718
200	.00766	.00201	.00117	.00981	.00385	.00496	.00180	.0115	.00125	.00438	.00171	.0503
300	.00509	.00137	.000829	.00704	.00280	.00366	.00135	.00876	.000953	.00340	.00134	.0367
400	.00343	.000967	.000601	.00518	.00208	.00276	.001202	.00679	.000741	.00269	.00107	.0274
500	.00239	.000683	.000440	.00388	.00157	.00212	.000791	.00535	.000585	.00216	.000808	.0208
600	.00169	.000496	.000333	.00292	.00120	.00163	.000616	.00425	.000466	.00175	.000709	.0161
700	.00120	.000364	.000247	.00222	.000919	.00127	.000482	.00343	.000373	.00143	.000582	.0126
800	.000769	.000267	.000187	.00170	.000715	.000962	.000385	.00274	.000301	.00116	.000481	.00969
900	.000619	.000148	.000143	.00133	.000558	.000789	.000307	.00169	.000244	.000966	.000399	.00772
1,000	.000423	.000148	.0000987	.00104	.000439	.000629	.000244	.00180	.000200	.000793	.000333	.00577

TABLE 5.—*Total flux and total intensities of various components from uranium elementary source emitting 1 photon per foot per second*

Altitude (feet)	Energy (Mev)										Total flux (photons per square foot per second)
	0.609	0.769	0.934	1.120	1.238	1.378	1.509	1.764	1.848	2.204	2.432	
	Total intensity (photons per square foot per second)											
100	6.58×10^{-7}	1.37×10^{-7}	8.05×10^{-8}	6.80×10^{-7}	2.62×10^{-7}	3.31×10^{-7}	1.19×10^{-7}	7.34×10^{-7}	7.88×10^{-8}	2.69×10^{-7}	1.03×10^{-7}	3.45×10^{-6}
200	1.35	.294	1.76	1.54	.597	.756	.271	1.70	1.84	.630	.243	.774
300	.503	.114	.714	.617	.241	.306	.113	.696	.754	.261	.102	.310
400	.144	.0553	.357	.352	.122	.157	.0567	.361	.391	.136	.0528	.151
500	.113	.0304	.202	.177	.0697	.0911	.0327	.212	.230	.0810	.0313	.0881
600	.0683	.0186	.124	.110	.0441	.0584	.0207	.134	.146	.0514	.0203	.0553
700	.0401	.0114	.0796	.0717	.0286	.0373	.0139	.0900	.0979	.0350	.0136	.0359

TABLE 6.—*Primary flux and primary intensities of various components from uranium elementary source emitting 1 photon per foot per second*

Altitude (feet)	Energy (Mev)										Primary flux (photons per square foot per second)
	0.609	0.769	0.934	1.120	1.238	1.378	1.509	1.764	1.848	2.204	2.432	
	Primary intensity (photons per square foot per second)											
100	2.96×10^{-7}	7.25×10^{-7}	3.98×10^{-8}	3.19×10^{-7}	1.23×10^{-7}	1.53×10^{-7}	5.49×10^{-8}	3.37×10^{-7}	3.63×10^{-8}	1.22×10^{-7}	4.66×10^{-8}	1.60×10^{-6}
200	.573	1.44	.807	.660	.255	.323	1.16	.724	.782	.268	1.03	.332
300	.198	.510	.294	.243	.0946	.121	.440	.277	.300	.104	.402	.123
400	.0731	.228	.135	.128	.0444	.0574	.210	.134	.146	.0512	.199	.0580
500	.0402	.116	.0706	.0597	.0237	.0310	.114	.0739	.0806	.0287	.112	.0307
600	.0231	.0641	.0400	.0343	.0137	.0181	.0672	.0441	.0483	.0174	.0686	.0180
700	.0131	.0375	.0240	.0208	.00839	.0112	.0419	.0279	.0306	.0112	.0444	.0110

TABLE 7.—*The function* G_3 *(500,ρ,a)*

ρ (feet)	a (feet)									
	400	500	600	700	800	900	1,000	1,500	2,000	2,500
0	0.8390	1.0962	1.3147	1.4931	1.6351	1.7475	1.8354	2.0557	2.1170	2.1321
100	.7856	1.0558	1.2899	1.4797	1.6286	1.7445	1.8336	2.0553	2.1167	2.1318
200	.7152	.9883	1.2325	1.4340	1.5935	1.7177	1.8132	2.0500	2.1153	2.1312
300	.6279	.8937	1.1427	1.3560	1.5297	1.6673	1.7742	2.0398	2.1126	2.1304
400	.5236	.7720	1.0203	1.2457	1.4373	1.5932	1.7165	2.0248	2.1087	2.1294
500	.4023	.6232	.8654	1.1031	1.3162	1.4954	1.6402	2.0049	2.1036	2.1281
600	.2962	.4785	.6979	.9344	1.1637	1.3677	1.5379	1.9783	2.0964	2.1274
700	.2122	.3533	.5368	.7543	.9860	1.2090	1.4061	1.9416	2.0870	2.1246
800	.1500	.2543	.3977	.5816	.7972	1.0254	1.2437	1.8937	2.0750	2.1191
900	.1055	.1806	.2875	.4324	.6164	.8306	1.0561	1.8312	2.0588	2.1160
1,000	.0743	.1277	.2052	.3138	.4597	.6438	.8570	1.7482	2.0374	2.1138
1,100	.0582	.1001	.1608	.2461	.3614	.5084	.6825	1.5770	2.0318	2.1010
1,200	.0442	.0759	.1219	.1867	.2750	.3894	.5285	1.4098	2.0036	2.0881
1,300	.03207	.0551	.0885	.1357	.2007	.2867	.3950	1.2466	1.9528	2.0753
1,500	.0138	.0237	.0380	.0586	.0882	.1303	.1899	.9320	1.7835	2.0496
2,000	.0027	.0047	.0075	.0116	.0173	.0255	.0369	.2150	.9649	1.7962
2,500					.0032	.0049	.0072	.0426	.2282	.8827
3,000								.0080	.0457	.2362
3,500									.0085	.0478
4,000										.0088

TABLE 8.—*The function* G_1 *(500,y,a)*

y (feet)	a (feet)									
	400	500	600	700	800	900	1,000	1,500	2,000	2,500
0	0.8086	0.9780	1.1303	1.2655	1.3843	1.4879	1.5778	1.8720	2.0098	2.0727
400	.4569	.5784	.7027	.8287	.9543	1.0773	1.1955	1.6602	1.9095	2.0263
500	.3496	.4470	.5500	.6584	.7715	.8877	1.0051	1.5267	1.8422	1.9966
600	.2621	.3372	.4183	.5061	.6007	.7021	.8091	1.3569	1.7489	1.9532
700	.1946	.2511	.3129	.3809	.4559	.5384	.6286	1.1583	1.6246	1.8909
800	.1439	.1859	.2322	.2835	.3408	.4049	.4766	.9478	1.4657	1.8076
900	.1063	.1375	.1718	.2100	.2529	.3013	.3562	.7466	1.2748	1.6976
1,000	.0787	.1017	.1270	.1553	.1871	.2232	.2643	.5714	1.0638	1.5543
1,500	.0177	.0228	.0284	.0347	.0417	.0496	.0587	.1291	.2767	.5766
2,000	.0036	.0047	.0059	.0072	.0087	.0104	.0124	.0279	.0604	.1292
2,500					.0010	.0013	.0017	.0048	.0118	.0271
3,000										.0041

TABLE 9.—*The function G_4 (500,z,a)*

z (feet)	a (feet)									
	400	500	600	700	800	900	1,000	1,500	2,000	2,500
0	2.0395	2.9588	3.9346	4.9385	5.9824	7.0540	8.1419	13.1905	18.1905	23.0945
100	1.9134	2.8337	3.8268	4.8469	5.9096	6.9872	8.0807	13.1576	18.3635	23.0731
200	1.7513	2.6455	3.6313	4.6534	5.7248	6.8081	7.9094	13.0481	18.2865	23.0079
300	1.5530	2.3941	3.3480	4.3579	5.4279	6.5168	7.6279	12.8622	18.1511	22.8988
400	1.3186	2.0796	2.9770	3.9605	5.0191	6.1133	7.2363	12.5997	17.9573	22.7459
500	1.0481	1.7019	2.5182	3.4611	4.4983	5.5975	6.7345	12.2607	17.7051	22.5491
600	.8049	1.3398	2.0450	2.9096	3.9037	4.9849	6.1324	11.8389	17.3894	22.3036
700	.6063	1.0241	1.6010	2.3549	3.2663	4.3063	5.4361	11.3264	17.0114	22.0047
800	.4509	.7709	1.2224	1.8406	2.6318	3.5872	4.6735	10.7206	16.5624	21.6649
900	.3343	.5745	.9211	1.4029	2.0571	2.8886	3.8868	10.0076	16.0254	21.2993
1,000	.2475	.4261	.6857	1.0496	1.5667	2.2501	3.1170	9.1951	15.4124	20.8783
1,100	.1972	.3393	.5461	.8364	1.2496	1.7994	2.5058	8.0093	14.6867	20.4541
1,200	.1529	.2627	.4230	.6484	.9699	1.4014	1.9648	6.9047	13.8871	19.9409
1,300	.1144	.1964	.3164	.4856	.7275	1.0561	1.4940	5.8811	13.0136	19.3386
1,500	.0554	.0946	.1527	.2354	.3547	.5234	.7632	4.0773	11.0450	17.8670
2,000	.0016	.0198	.0323	.0505	.0764	.1133	.1658	.9870	4.8304	12.6298
2,500					.0123	.0202	.0308	.2091	1.1628	5.4713
3,000								.0348	.2425	1.3130
3,500									.0382	.2728
4,000										.0420

TABLE 10.—*Ratio of grade-area predicted from elementary source relation to actual grade-area as function of radius, a, and ground projection, z, of closest distance of approach*

z (feet)	a (feet)						
	400	500	600	700	800	900	1,000
0	2.32	2.98	4.08	5.46	7.34	9.78	13.10
100	2.04	2.82	3.85	5.50	7.07	9.42	12.60
200	1.91	2.61	3.56	4.80	6.56	8.89	12.00
300	1.76	2.36	3.19	4.34	5.98	8.09	11.00
400	1.61	2.10	2.82	3.78	5.20	7.01	9.65
500	1.55	1.80	2.36	3.15	4.26	5.62	8.13
600	1.29	1.55	1.95	2.58	3.48	4.78	6.73
700	1.18	1.37	1.65	2.11	2.79	3.80	5.25
800	1.06	1.21	1.39	1.73	2.22	2.82	4.10
900	.945	1.07	1.22	1.45	1.81	2.31	3.13
1,000	.877	.994	1.08	1.22	1.48	1.84	2.40
1,100	.672	.808	.904	1.01	1.25	1.54	2.00
1,200	.627	.685	.788	.867	1.04	1.29	1.84
1,300	.494	.559	.634	.724	.852	1.05	1.34

TABLE 11.—*Ratio of elementary source grade-area to actual grade-area averaged over two flight lines as function of radius, a, and ground projection, z, of closest distance of approach*

z (feet)	a (feet)						
	400	500	600	700	800	900	1,000
0	1.40	1.76	2.35	3.09	4.09	5.41	7.20
100	1.38	1.75	2.32	3.01	4.05	5.35	7.20
200	1.29	1.71	2.23	2.91	3.91	5.16	7.00
300	1.32	1.72	2.13	2.78	3.73	4.96	6.70
400	1.24	1.58	2.02	2.61	3.50	4.66	6.39
500	1.30	1.50	1.88	2.44	3.24	4.22	6.11
600	1.23	1.46	1.85	2.35	3.13	4.29	5.99

TABLE 12.—*Conversion factors to correct elementary source grade-area prediction to true grade-area for finite sources. Minimum and maximum columns show extreme spread in factors*

a (feet)	Minimum	Average	Maximum	a (feet)	Minimum	Average	Maximum
0	1. 000	1. 000	1. 000	700	0. 324	0. 368	0. 425
400	. 714	. 765	. 813	800	. 244	. 276	. 319
500	. 568	. 613	. 684	900	. 185	. 207	. 233
600	. 426	. 477	. 540	1,000	. 139	. 151	. 167

TABLE 13.—*Ratio of total counts, $H_f(500,z,a)$, to peak intensity, $I_f(500,z,a)$, as function of radius, a, and ground projection, z, of the closest distance of approach for finite source*

z (feet)	a (feet)							
	0	400	500	600	700	800	900	1,000
0	3. 74	4. 86	5. 40	5. 99	6. 62	7. 32	8. 07	8. 87
100	3. 76	4. 70	5. 37	5. 93	6. 55	7. 26	8. 01	8. 81
200	3. 93	4. 90	5. 35	5. 89	6. 49	7. 19	7. 93	8. 72
300	4. 16	4. 95	5. 36	5. 86	6. 43	7. 10	7. 80	8. 60
400	4. 51	5. 04	5. 39	5. 84	6. 36	6. 98	7. 67	8. 43
500	4. 89	5. 21	5. 46	5. 82	6. 28	6. 84	7. 49	8. 21
600	5. 22	5. 43	5. 60	5. 86	6. 23	6. 71	7. 29	7. 98
700		5. 71	5. 80	5. 96	6. 24	6. 63	7. 12	7. 73
800		6. 01	6. 06	6. 15	6. 33	6. 60	7. 00	7. 52
900		6. 34	6. 36	6. 41	6. 49	6. 67	6. 96	7. 36
1,000		6. 66	6. 67	6. 68	6. 69	6. 82	6. 99	7. 27
1,100		6. 78	6. 78	6. 79	6. 80	6. 92	7. 08	7. 34
1,200		6. 92	6. 92	6. 94	6. 95	7. 05	7. 20	7. 44
1,300		7. 13	7. 13	7. 15	7. 16	7. 25	7. 37	7. 56

TABLE 14.—*Ratio of total counts, $H_s(500,0,a)$ at normal incidence, to peak intensity, $I_s(500,0,a)$, as function of width, a, of a slab source*

a (feet)	H_s/I_s	a (feet)	H_s/I_s
0	4. 36	900	5. 73
400	4. 68	1,000	6. 00
500	4. 82	1,500	7. 58
600	5. 02	2,000	9. 38
700	5. 24	2,500	11. 30
800	5. 47		